

**MATERIAL CHARACTERIZATION AND LIFE PREDICTION OF A  
CARBON FIBER/THERMOPLASTIC MATRIX COMPOSITE FOR USE IN  
NON-BONDED FLEXIBLE RISERS**

Blair Edward Russell

A thesis submitted to the Faculty of the Virginia Polytechnic Institute and State University in  
partial fulfillment of the requirements for the degree of

Master of Science

In

Engineering Mechanics

Kenneth L. Reifsnider, Chair

Scott W. Case, Co-chair

John J. Lesko

December 12, 2000

Blacksburg Virginia

**Keywords:** polymer matrix composite (PMC), polyphenylene sulfide (PPS), bend-rupture,  
semicrystalline polymers, crystallinity

Copyright 2000, Blair Edward Russell

**MATERIAL CHARACTERIZATION AND LIFE PREDICTION OF A  
CARBON FIBER/THERMOPLASTIC MATRIX COMPOSITE FOR USE IN  
NON-BONDED FLEXIBLE RISERS**

**Blair Edward Russell**

**(ABSTRACT)**

In the effort to improve oil production riser performance, new materials are being studied. In the present case, a Polymer Matrix Composite (PMC) is being considered as a replacement for carbon steel in flexible risers manufactured by Wellstream Inc., Panama City, Florida. The Materials Response Group (MRG) at Virginia Tech had the primary responsibility to develop the models for long-term behavior, especially remaining strength and life. The MRG is also responsible for the characterization of the material system with a focus on the effects of time, temperature, and environmental exposure. The present work is part of this effort. The motivation to use a composite material in a non-bonded flexible riser for use in the offshore oil industry is put forth. The requirements for such a material are detailed. Strength analysis and modeling methods are presented with experimental data. The effect of matrix crystallinity on composite mechanical properties is shown. A new method for investigating matrix behavior at elevated temperatures developed. A remaining strength life prediction methodology is recalled and applied to the case of combined fatigue and rupture loading.

## **DEDICATION**

This work is dedicated to my family David, Raylene, and Erika, who never let me limit my expectations.

## ACKNOWLEDGMENTS

There are many who contributed to this work; I would like to acknowledge the following:

**Dr. Kenneth Reifsnider-** Aside from serving as my committee chair, Dr. Reifsnider has provided mentorship and given me opportunities that I likely would not have had if not for his insight and his faith in me. I thank him for giving me the opportunity to teach and “run” my own project, and for the support he provided in my effort to become a graduate student.

**Dr. Scott Case-** Scott not only served as the Co-chair of my committee, but also gave me my start in the world of experimental mechanics. He has provided invaluable support to the life prediction work contained in this thesis and answered more than his share of questions concerning most every subject.

**Dr. Jack Lesko-** Jack served as a committee member and I must also thank him for the use of the environmental chamber and his advise on compression testing.

**Dr. Celine Mahieux** Celine contributed greatly to my work with the bend-rupture test method and made it just uncomfortable enough for me to make sure I published my first paper. I hope we have the chance to work together again.

**Dr. Nikhil Verghese-** Nikhil helped tremendously in the discovery of the role that crystallinity was playing in my results. I hope he becomes a professor.

**Sneha Patel-** Sneha helped me quite a bit at the end of this effort with DMA and other tests. Over the years she has also provided entertainment in the form of work breaks and encouragement (although not always constructive).

**Jolyn Senne -** Jolyn made sure the office was fun place to be, but most importantly I must thank her for her support, encouragement, and help making life-changing decisions.

**James Loverich-** James paved the way for me to work in Panama City Fl. with Wellstream. He also has contributed some of the experimental data presented here.

**Tozer Bandorawalla-** Tozer contributed to the strength modeling in the present work, was my early morning workout partner, and kept the MRG constantly entertained.

**Marshall “Mac” McCord-** In many ways Mac is the glue that keeps the experimental work together. He consistently provides quick and cheap solutions to complicated experimental problems. He is a wizard with the Sherline mill and lathe.

**Shelia Collins and Beverly Williams -** To call Shelia and Bev support personal is a bit of a misnomer. The success of the group is a function of the work that they do. They have helped me in many ways not the least of which is the moral support they have given in the difficult times.

**Dave Simmons and Darrel Young-** These guys have provided very quick turn around on so many critical fixtures and parts that would have taken the old machine shop guys forever. They have been a pleasure to deal with professionally, and I must also thank Dave for the venison and other homegrown goodies that he has sent my way.

**The Engineering Science and Mechanics Department -** I thank them for giving me a “home” and providing excellent administrative support throughout the years. In particular, Loretta Tickle, Pat Baker, Nancy Linkous, Wanda Roberts, Paul Siburt and Edmond Henneke made the tasks that could have been headaches, painless and efficient.

**The Materials Response Group-** The MRG has more or less been a home for me the past five years. Due mostly to the people involved, the working environment and camaraderie are unique. I hope that this is not the last time I am part of such a group.

# TABLE OF CONTENTS

<b>Acknowledgments</b> .....	<b>iii</b>
<b>Dedication</b> .....	<b>iii</b>
<b>List of Tables</b> .....	<b>viii</b>
<b>List of Figures</b> .....	<b>ix</b>
<b>1 Introduction and Literature review</b> .....	<b>1</b>
1.1 Introduction.....	1
1.2 Objective .....	1
1.3 Non-bonded Flexible Pipes .....	2
1.3.1 Requirements for Tensile Armor Materials .....	4
1.4 Composite Properties .....	5
1.4.1 Weibull Strength.....	6
1.4.2 Bundle Strength.....	8
1.4.3 Tensile Strength of Unidirectional Composites (Batdorf) .....	9
1.4.4 Other Models .....	10
1.5 Matrix Properties.....	10
1.5.1 Matrix Characterization.....	12
1.5.1.1 Dynamical Mechanical Analysis (DMA) .....	13
1.6 Bend-rupture.....	15
1.6.1 Bend-Rupture Fixture .....	17
1.6.2 Specimen Geometry .....	19
1.6.3 Analysis .....	19
1.7 Composite Life Prediction.....	23
1.8 Summary: Chapter 1.....	24
<b>2 Experimental Methods</b> .....	<b>26</b>
2.1 Quasi-Static Tensile Test .....	26
2.2 Tensile Rupture Test .....	32
2.3 Tension-Tension Fatigue Test.....	34
2.4 End-Loaded Bend Rupture Test .....	35
2.4.1 End-Loaded Bend Rupture Fixture .....	35
2.5 Dynamic Mechanical Analysis (DMA).....	36
2.6 Environmental Aging.....	37
2.7 Summary: Chapter 2.....	38
<b>3 The effects of temperature and processing history on Composite Mechanical Properties</b> .....	<b>40</b>
3.1 Composite and its Constituents .....	40
3.1.1 Fiber .....	40
3.1.2 Matrix .....	41

3.1.3	Constructing the Composite .....	42
3.2	Material From Run 1 and Run 2.....	43
3.2.1	Preliminary Tests Results.....	43
3.2.2	Quasi-Static Strength Data.....	44
3.2.3	Bend-Rupture Data .....	45
3.2.4	Dynamic Mechanical Analysis .....	47
3.2.4.1	Run 1 DMA.....	48
3.2.4.2	Run 2 DMA.....	49
3.2.5	Reprocessing Experiment.....	50
3.3	Additional Runs .....	52
3.4	Summary: Chapter 3.....	56
<b>4</b>	<b>Tensile Strength and Tensile Rupture Behavior .....</b>	<b>57</b>
4.1	Initial Tensile Strength.....	57
4.2	Weibull Tensile Strength Distribution .....	60
4.3	Tensile Rupture Behavior .....	63
	Summary: Chapter 4.....	65
<b>5</b>	<b>Fatigue – rupture combined loading.....</b>	<b>66</b>
5.1	Life Prediction Overview .....	67
5.2	Method Validation.....	71
5.2.1	Tensile Rupture.....	71
5.2.2	Fatigue .....	73
5.2.3	Combined Rupture and Fatigue .....	74
5.3	R-Ratio Influence.....	75
5.4	Summary: Chapter 5.....	76
<b>6</b>	<b>Conclusions .....</b>	<b>77</b>
	<b>References.....</b>	<b>79</b>
	<b>Vita .....</b>	<b>83</b>

## LIST OF TABLES

Table 1-1 Requirements for tensile armor material properties .....	5
Table 1-2 Comparison between typical steel and Carbon/PPS Composite properties .....	6
Table 1-3 Neat PEEK 150P properties as a function of crystallinity .....	12
Table 2-1 Tests methods and procedures.....	39
Table 3-1 Typical properties of Grafil 34-700 carbon fiber .....	41
Table 3-2 Typical room temperature (25°C) mechanical properties of PPS.....	41
Table 3-3 Typical room temperature physical properties of PPS .....	42
Table 3-4 Comparison of room temperature Run 1 and Run 2 properties.....	44
Table 3-5 Run 1 tensile properties at temperature and post aging .....	45
Table 3-6 Processing parameter definitions.....	53
Table 3-7 Samples 1-9 processing parameters .....	54
Table 3-8 Quasi-static test results .....	54
Table 4-1 Weibull reference strength for various gage lengths.....	58
Table 4-2 Strength models compared to experimental results.....	59

**LIST OF FIGURES**

Figure 1-1 Typical flexible riser installation..... 2

Figure 1-2 Typical flexible riser structure ..... 3

Figure 1-3 End-loaded bending condition..... 17

Figure 1-4 End-loaded bend rupture fixture..... 18

Figure 1-5 Pinned-pinned post-buckling loading condition ..... 19

Figure 1-6 Normalized strain vs. fixture length ..... 22

Figure 2-1 Typical tensile specimen and tabbing ..... 27

Figure 2-2 Typical quasi-static tensile test load-time trace..... 28

Figure 2-3 Typical quasi-static tensile test stress-strain curve ..... 29

Figure 2-4 Measured quasi-static tensile strength versus loading rate..... 30

Figure 2-5 MTS load frame with box heater..... 31

Figure 2-6 Load frame and environmental chamber ..... 32

Figure 2-7 Typical tensile rupture test load-time trace ..... 33

Figure 2-8 Typical tension-tension fatigue test load-time trace..... 34

Figure 2-9 End-loaded bend rupture fixture..... 36

Figure 2-10 Typical DMA plot ..... 37

Figure 3-1 Schematic of composite tape pultrusion manufacturing process..... 43

Figure 3-2 90 °C Bend-rupture results for Run 1 and Run 2 ..... 46

Figure 3-3 Representative DMA of Run 1 as received.....	48
Figure 3-4 Representative DMA of batch 2 as received.....	49
Figure 3-5 DMA of batch 1 as modified.....	51
Figure 3-6 DMA of batch 2 as modified.....	52
Figure 3-7 90 °C Bend-rupture results for Samples 4, 5, 6 and Run 1 and Run 2.....	55
Figure 4-1 Probability of failure for material from 1 run of the carbon fiber/PPS composite as received .....	61
Figure 4-2 Probability of failure for material from 6 runs of the carbon fiber/PPS composite as received and aged.....	62
Figure 4-3 Comparison of probability of failure for three cases.....	63
Figure 4-4 Time to rupture at temperature .....	64
Figure 5-1 The use of remaining strength as a damage metric .....	68
Figure 5-2 Tensile rupture curve fit and data.....	72
Figure 5-3 Room temperature fatigue data and S-N curve fit .....	74
Figure 5-4 Comparison of elevated temperature fatigue prediction and 90°C fatigue data .....	75

# Chapter 1

## 1 INTRODUCTION AND LITERATURE REVIEW

### 1.1 Introduction

In the effort to improve oil production riser performance, new materials are being studied. In the present case, a polymer matrix composite (PMC) is being considered as a replacement for carbon steel in flexible risers manufactured by Wellstream Inc., Panama City, Florida [1, 2]. The Materials Response Group (MRG) at Virginia Tech has the primary responsibility to develop the models for long-term behavior, especially remaining strength and life. The MRG is also responsible for the characterization of the material system with a focus on the effects of time, temperature, and environmental exposure. The present work is part of this effort.

### 1.2 Objective

The objective of this thesis is to present several key findings produced during the research and development of a carbon fiber/thermoplastic matrix composite intended to replace a steel component in a non-bonded flexible riser. These findings include the introduction of a test method that proves to be simple to implement and sensitive to subtle differences in the matrix material of composites. In addition, the importance of manufacturing processing parameters on the long-term behavior of a semicrystalline thermoplastic matrix composite will be illuminated. Experimentally determined static strength, fatigue behavior at room and elevated temperatures, and tensile rupture data are presented as a basis for future life

prediction modeling. A remaining strength approach for life prediction will be developed and presented for the case of combined fatigue and rupture loading.

### **1.3 Non-bonded Flexible Pipes**

Non-Bonded Flexible Pipes (NFP) have been used in the offshore oil industry for over 30 years. These pipes, when used in deepwater, function as risers that bring high pressure and temperature production fluid (raw oil and gas) from the seabed to floating production vessels on the ocean surface. Figure 1-1 shows a simplified riser installation.

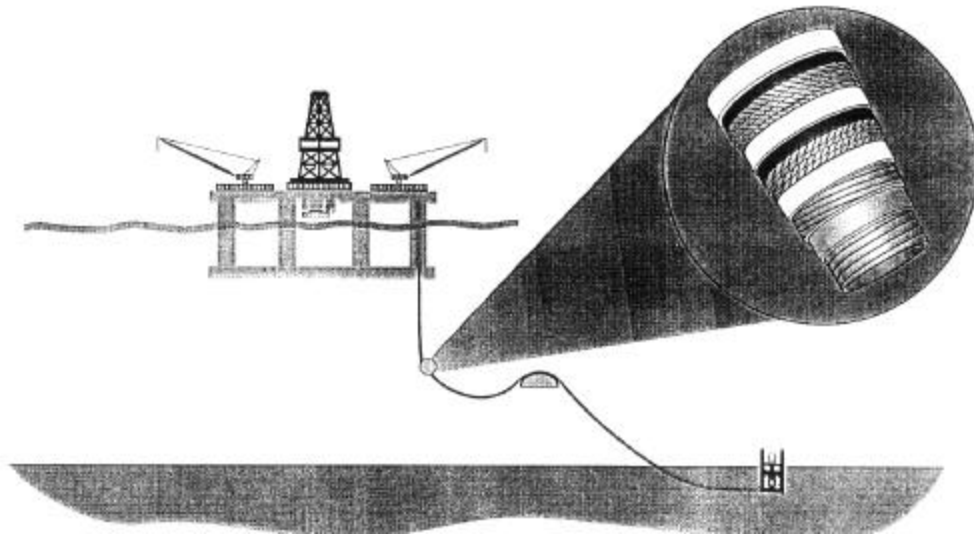


**Figure 1-1 Typical flexible riser installation (detail shows pipe structure)**

These pipes are constructed of many layers made up of several material types. Each of these layers is intended to perform a specific function. The structure of a non-bonded flexible pipe is illustrated in Figure 1-2. These layers are allowed to slide with respect to one another, which allows the structure to be flexible. The flexibility of the structure allows long

continuous lengths of pipe to be manufactured, stored, transported, deployed and recovered from reels. Depending on the diameter of the pipe, continuous lengths of up to 2 miles can be placed on a single reel. In many service applications, this represents a considerable advantage over competing technologies that require many short segments to be connected to obtain long pipelines. Materials in a conventional NFP consist of steel and thermoplastic polymers. Steel is used primarily for load-bearing elements in the tensile strength, hoop strength, and collapse resistant layers. Thermoplastic polymers are used mainly as fluid barriers and to prevent wear.

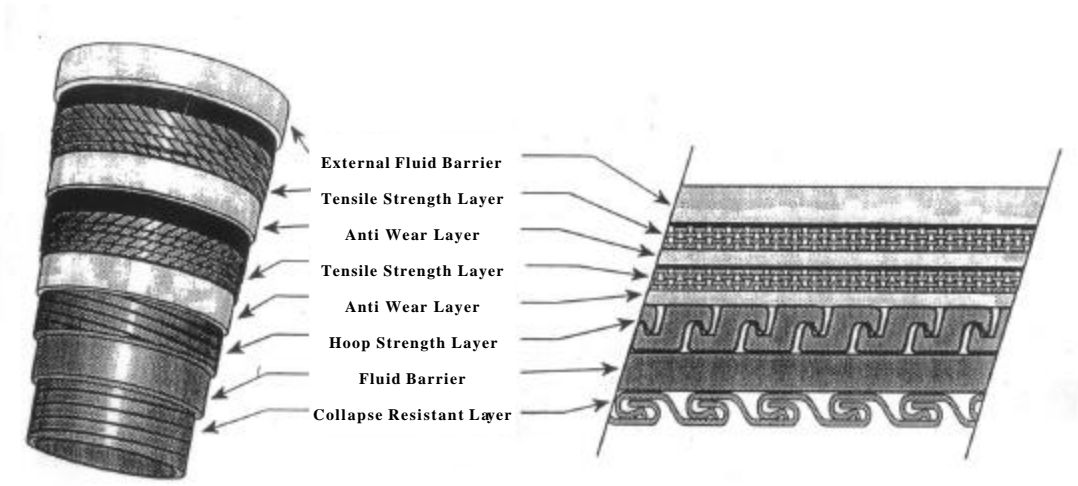


**Figure 1-2 Typical flexible riser structure**

The present work concentrates on the tensile armor layers. Within the non-bonded flexible pipe industry (in this work as well), these layers are referred to as the tensile armor, which is somewhat misleading as its main function is to support the axial tensile loads on the structure. The tensile armor in a conventional NFP consists of two helically wound layers that are wound in opposing directions. Each of these layers is comprised of 50-70 rectangular steel wires. The tensile armor wires are laid at angles from  $\pm 25$  to  $\pm 40$  degrees to the axis of the

pipe. The counter wound layers, when designed properly, prevent torsion of the pipe caused by axial loads.

As the demands for oil continue to increase and oil reserves in shallow water are being exhausted, oil producers are forced into deeper water in order to access new reserves. Currently, the longest risers are about 6000 feet in length. The use of risers in deeper water requires the structure to support increasing axial tensile loads due to the hanging weight of the riser itself. For a given pipe design, the weight per unit length of a steel armored riser limits the depth of water in which it can operate. As the hanging length of the riser is increased it will eventually fail under its own weight. This poses an engineering challenge in the effort to reach oil reserves in ultra deep water and motivates the development of risers with increased axial strength and decreased weight. A logical solution is to replace the tensile armor with a material with greater specific strength (i.e. strength per unit mass).

### **1.3.1 Requirements for Tensile Armor Materials**

Because the riser is hanging vertically the tensile armor wires are subjected to static tensile loads due to its own weight, dynamic bending loads due to the surface vessel motion in waves, axial loads due to internal pressure, vibratory loads due to vortex shedding in currents, as well as exposure to elevated temperatures and aggressive chemicals. Loads on a single tensile armor wires can be simplified to static tensile loads, cyclic tensile loads, and exposure elevated temperatures and chemicals. Table 1-1 lists the requirements set by Wellstream [1] for tensile armor material properties.

**Table 1-1 Requirements for tensile armor material properties**

<b>Property</b>	<b>Requirement</b>
Initial Strength	180 ksi (minimum)
Flexibility	6.0 in (minimum) bend radius at 0.04 in (minimum) thickness
Allowable Utilization-Static	50% of initial strength
Allowable Utilization-Dynamic	40% of initial strength
Density (max)	1.6 S.G.
Temperature Range (pipe annulus)	-40 to 93°C
Environmental	Seawater, 5000 ppm H <sub>2</sub> S and 5% CO <sub>2</sub> in pipe bore
Cost	Finished pipe cost no more than 25% greater than conventional of same performance

Numerous fiber/polymer composites were considered in the early stages of the material selection effort. Because of the aggressive service environment and the stiffness requirements many materials were eliminated. A unidirectional carbon fiber/ polyphenylene sulfide (PPS) matrix composite was chosen as the best candidate to replace the steel tensile armor.

#### **1.4 Composite Properties**

It is well understood that composites behave differently than most metals. This is certainly case with the chosen material. A ductile steel is being replaced with a brittle composite. This difference presents several design challenges and the characteristics of composite behavior need to be reviewed. As a point of reference, Table 1-2 presents a comparison of properties between the composite and the steel it replaces.

**Table 1-2 Comparison between typical steel and Carbon/PPS Composite properties [1]**

	<b>Steel</b>	<b>Carbon/PPS</b>
Strength	110 ksi	180 ksi
Modulus	30 Msi	11.7 Msi
Elongation	<11%	1.40%
Relative Density	1	0.19
Relative Cost	1	2.5

### 1.4.1 Weibull Strength

Of key importance to the present work is the nature of composite strength. It was found that the strength distribution of unidirectional composites is often well represented by a Weibull statistical distribution [3]. The two parameter Weibull distribution differs from other statistical schemes in that the values described range from zero to positive infinity, which makes more physical sense for strength than a distribution that ranges for negative infinity to positive infinity. Weibull statistics are based on the probability of encountering a flaw that will cause failure at a given stress over a given length of a load-bearing member. The following is a brief description of Weibull statistics adapted from the work of Case [3].

If we apply Weibull statistics to a member of length  $L$ , the cumulative number of defects which can fail at stress  $\mathbf{s}$  is given by

$$\Phi(L, \mathbf{s}) = \frac{L}{L_0} \left( \frac{\mathbf{s}}{\mathbf{s}_0} \right)^m \quad (1)$$

We may interpret the parameters  $L_0$  and  $\mathbf{s}_0$  by recognizing that  $\mathbf{s}_0$  is the stress required to cause one failure, on average, in a member of length  $L_0$ . The parameter  $m$ , the Weibull modulus, describes the amount of variability (the scatter) in the strength values about the

average (large values of  $m$  correspond to small amounts of scatter in the data). We may relate  $\Phi$  to the measured (experimental) probability of failure by

$$\begin{aligned} P_f(L, \mathbf{s}) &= 1 - \exp[\Phi(L, \mathbf{s})] \\ &= 1 - \exp\left[-\frac{L}{L_0}\left(\frac{\mathbf{s}}{\mathbf{s}_0}\right)^m\right] \end{aligned} \quad (2)$$

The corresponding reliability,  $R(L, \mathbf{s})$  is given by

$$\begin{aligned} R(L, \mathbf{s}) &= 1 - P_f(L, \mathbf{s}) \\ &= \exp\left[-\frac{L}{L_0}\left(\frac{\mathbf{s}}{\mathbf{s}_0}\right)^m\right] \end{aligned} \quad (3)$$

Note: Because Equations (1) and (2) depend upon the length  $L$ , values for  $\mathbf{s}_0$  and  $m$  must always be quoted (or determined) at a reference value of  $L_0$

Two different means are available for us to determine  $m$  and  $\mathbf{s}_0$ . Unfortunately each of these methods involves testing large numbers of specimens. In the first method, many specimens are tested at a fixed gage length. The resulting strength values are fit to a Weibull distribution. This process is repeated at other gage lengths, so that new values for  $m$  and  $\mathbf{s}_0$  are obtained. The values for  $\mathbf{s}_0$  are converted to one reference length by using the relation

$$\mathbf{s}_0 = \mathbf{s}_{02} \left(\frac{L_{02}}{L_0}\right)^{\frac{1}{m}} \quad (4)$$

Ideally these values for  $m$  and  $\sigma_0$  would be identical. In practice, however, the values are different. The common procedure is then to average the resulting values for  $m$  and  $\mathbf{s}_0$ .

However, numerical simulations suggest that a better method is available. In this method, one proceeds, as before, determining  $\mathbf{s}_0$  at different gage lengths, only in this case the values are not converted to a common reference length. Rather, a linear regression is performed on the  $\log(\mathbf{s}_0)$  versus  $L_0$ . From the form of Equation (4), we can see that such a plot should have slope of  $-\frac{1}{m}$ . The resulting line may also be used to determine  $\mathbf{s}_0$ .

While Weibull distributions fit unidirectional composite strength data well, more fundamentally, they are a powerful tool in describing the strength of single fibers. Weibull statistics form the basis for the estimation of unidirectional composite tensile strength.

### 1.4.2 Bundle Strength

Using a Weibull distribution to describe the strength of single fibers, the interaction between many fibers under load can modeled and the estimation of the strength of a unidirectional composite can be made. As a first attempt, the composite can be thought of as bundle of fibers with no contribution to the strength from the matrix. Again adapted from Case [3] a bundle strength model is presented.

We begin with a bundle of fibers of length  $L$  whose strain-to-failures may be represented in terms of the Weibull parameters  $\mathbf{e}_0$  and  $m$  at a reference length  $L_0$  (the reason for choosing the strain-to-failure rather than the strength will become obvious shortly). The resulting reliability may be written as

$$R(\mathbf{e}) = \exp \left[ -\frac{L}{L_0} \left( \frac{\mathbf{e}}{\mathbf{e}_0} \right)^m \right] \quad (5)$$

The stress carried by the fibers at a given strain  $\mathbf{e}$  is given by

$$\mathbf{s} = E_f \mathbf{e} R(\mathbf{e}) \quad (6)$$

In order to estimate the strength of the bundle, we find the maximum of Equation (6) by setting  $\frac{d\mathbf{s}}{d\mathbf{e}} = 0$  and solving for  $\mathbf{e}$ . This critical value of  $\mathbf{e}$ ,  $\mathbf{e}_c$  is given by

$$\mathbf{e}_c = \mathbf{e}_0 \left( \frac{L_0}{mL} \right)^{\frac{1}{m}} \quad (7)$$

Substituting this value into Equation (6), we obtain the maximum fiber stress,

$$\mathbf{s}_{fc} = E_f \mathbf{e}_0 \left( \frac{L_0}{mLe} \right)^{\frac{1}{m}} \quad (8)$$

The corresponding composite stress is then given by

$$X_t = V_f E_f \mathbf{e}_0 \left( \frac{L_0}{mLe} \right)^{\frac{1}{m}} \quad (9)$$

where  $V_f$  is the fiber volume fraction of the composite.

### 1.4.3 Tensile Strength of Unidirectional Composites (Batdorf)

In a logical progression, the influence of having a matrix present was considered by Batdorf [4,5]. In his model, he considers the only damage in the composite to be fiber failure. The matrix only contributes as a means to introduce a stress concentration on adjacent fibers over an ineffective length. As load increases on the composite, the weakest fiber fails and sheds its stress to its neighbors increasing the probability that a neighboring fiber, in the plane of the initial break, will fail. The single fiber break (singlet) becomes a double fiber break

(doublet) and so on. As the load is increased this process continues to the point of instability and ultimate failure of the composite. The lowest stress at which an arbitrary number of broken fibers becomes unstable defines the strength of the composite.

#### **1.4.4 Other Models**

More complex models have been developed in an effort to better represent experimental results and the underlying physics. These models make more specific assumptions as to interactions between broken fibers and the surrounding fibers.

Monte Carlo simulations for the strength of unidirectional polymer matrix composites [6] have been gaining acceptance. Like the bundle strength and Batdorf models, Monte Carlo simulations require the Weibull statistics for the strength of the fibers, in addition these simulations require the modulus of the fiber and matrix, the fiber volume fraction, fiber diameter, and packing arrangement as inputs. The Batdorf technique and the Monte Carlo simulations often produce over-estimates of composite strength when compared to experimental data. Although the Batdorf results are closer to the experimental strength, the Monte Carlo strength simulations more accurately mimic the progression of fiber breaks leading up to composite failure. In the Batdorf analysis, the breaks are assumed to be coplanar. This limitation is not imposed in the Monte Carlo simulations. An additional feature of the Monte Carlo simulations is that it yields Weibull statistics for failure of the composite from the fiber Weibull strength distribution.

### **1.5 Matrix Properties**

In general, the matrix plays two roles in the behavior of the composite. The matrix protects the fibers from the environment, and provides the path for load sharing between fibers. This second role is governed by parameters such as matrix stiffness, fracture toughness and the

interfacial bond characteristics between the matrix and fiber. A maximum in strength, for example, has been postulated by Gao [7] as a function of interfacial shear strength. Further, if matrix properties are variable or are dependent on environmental factors to which the composite is exposed, it would be expected that this change in matrix properties would be reflected in the composite behavior.

Of particular importance to the present study is the stiffness change in semicrystalline polymers due to temperature. An extensive review of the relaxation processes in semicrystalline polymers is given by Boyd [8,9]. He describes the relaxations  $\alpha$ ,  $\beta$ ,  $\gamma$  (labeled in order of decreasing temperature) that can occur in semicrystalline polymers. In polymers that possess all three relaxations, the  $\alpha$  relaxation is commonly considered to be connected with the crystalline phase of the polymer, in this case the  $\beta$  relaxation is associated with the amorphous phase and the temperature at which this relaxation occurs is referred to as the glass transition temperature,  $T_g$ , of the polymer.

Mahieux et al [10] noted that in the axial direction, the stiffness change of a carbon fiber polymer matrix composite was found to be more than 5%. The strength of the material dropped by 20% when the matrix underwent its glass transition.

While little literature exists that address the relationship between PPS properties and the behavior of PPS based composites, some literature exists that reports this relationship for PEEK and its composite. Both PPS and PEEK are semicrystalline thermoplastic polymers and exhibit similar behavior. Talbott et al [11] presents mechanical properties as a function of crystallinity and crystallinity is shown to depend on the cooling rate during manufacture. For the case of neat PEEK 150P, crystallinity varies from about 40% for cooling rates near 0.0° F/min to about 3% for cooling rates near 10,000 F/min. Further, tensile strength and modulus, shear strength and modulus, compressive strength, and mode I fracture toughness are reported as functions of crystallinity. Table 1-3 summarizes Talbott's findings.

**Table 1-3 Neat PEEK 150P properties as a function of crystallinity [11]**

<b>Property</b>	<b>@ 15% Crystallinity</b>	<b>@ 40% Crystallinity</b>	<b>Change (%)</b>
Tensile modulus (ksi)	500	650	23
Tensile strength (ksi)	10	14	29
Shear modulus (ksi)	175	200	13
Shear strength (ksi)	6	9	33
Compression strength (ksi)	22	25	12
Fracture toughness, mode I (ksi in <sup>0.5</sup> )	10	3	-70

The data in Table 1-3 indicate that, in general, neat PEEK properties increase with degree of crystallinity. The exception to this trend is the mode I fracture toughness. This property decreases 70% from its value at 15% crystallinity.

The fracture toughness and fracture energy of an APC-2 (carbon fiber/PEEK matrix) composite was also investigated by Talbott. The mode one fracture toughness and fracture energy decreased over a range of matrix crystallinity from 0 to 35%. These decreases were 32% and 15% respectively. Other properties were not studied.

The literature generally does not address the effect of semicrystalline thermoplastic matrix properties on fiber direction composite properties. It is assumed that the fibers dominate the behavior of the material so little attention need be paid to the matrix properties. The present work seeks to challenge this thinking.

### **1.5.1 Matrix Characterization**

It has been shown that matrix behavior contributes to the behavior of the composite. In order to relate matrix properties to composite properties, the matrix must be characterized. Two methods will now be reviewed that assess the effects of time and temperature on matrix behavior. The first is a standard and excepted method, the Dynamic Mechanical Analysis

(DMA), the second is a method developed by the author and colleagues. Although the bend-rupture method development is original work it is presented here as support of Chapter 3.

### 1.5.1.1 Dynamical Mechanical Analysis (DMA)

To characterize the viscoelastic behavior of the composite in this work, DMA's are performed. Descriptions of this standard test method can be found in many texts [12], the following discussion is a review of the method. A DMA consists of forcing an alternating displacement on a specimen and measuring the corresponding stress. For linear viscoelastic materials in equilibrium, the stress and strain vary sinusoidally, but the strain lags the stress, i.e., when trying to displace the specimen the stress increases before the strain. The strain  $\epsilon$  and stress,  $\sigma$ , can be written as

$$\mathbf{e} = \mathbf{e}_o \sin \omega t \quad (10)$$

$$\mathbf{s} = \mathbf{s}_o \sin(\omega t + \mathbf{d}) \quad (11)$$

respectively, where  $\omega$  is the angular frequency,  $\delta$  is the phase lag. The stress can be further expanded.

$$\mathbf{s} = \mathbf{s}_o \sin \omega t \cos \mathbf{d} + \mathbf{s}_o \cos \omega t \sin \mathbf{d} \quad (12)$$

The stress is now written in two parts. The magnitude of stress in phase with the strain is given by  $\mathbf{s}_o \cos \mathbf{d}$  and the magnitude of stress that is 90 degrees out of phase with the strain is given by  $\mathbf{s}_o \sin \mathbf{d}$ . We can now define two quantities  $G_1$  and  $G_2$  to represent the stress-strain relationship in phase and out of phase respectively. This relationship is written as follows:

$$\mathbf{s} = \mathbf{e}_o G_1 \sin \omega t + \mathbf{e}_o G_2 \cos \omega t \quad (13)$$

Where

$$G_1 = \frac{\mathbf{S}_o}{\mathbf{e}_o} \cos \mathbf{d} \quad (14)$$

$$G_2 = \frac{\mathbf{S}_o}{\mathbf{e}_o} \sin \mathbf{d} \quad (15)$$

A complex modulus is defined as  $G^* = G_1 + G_2$ , and we will now call  $G_1$  the storage modulus and  $G_2$  the loss modulus. The storage modulus describes the energy stored as strain in the specimen. The loss modulus defines the energy lost during a cycle. This loss is given by

$$\Delta E = \int_0^{2p/w} \mathbf{S} \frac{de}{dt} dt \quad (16)$$

If substitutions are made for  $\sigma$  and  $\epsilon$ , the energy loss can be written

$$\Delta E = w \mathbf{e}_o^2 \int_0^{2p/w} (G_1 \sin wt \cos wt + G_2 \cos^2 wt) dt \quad (17)$$

through the application of trigonometric identities the integral 17 once evaluated gives

$$\Delta E = p G_2 \mathbf{e}_o^2 \quad (18)$$

if the integral 17 is evaluated for only one quarter cycle the first term yields

$$\Delta E = G_1 w \mathbf{e}_o^2 \int_0^{p/2w} \sin wt \cos wt dt \quad (19)$$

the maximum stored elastic energy,  $E$ , where

$$E = \frac{1}{2} G_1 \mathbf{e}_o^2 \quad (20)$$

is independent of frequency. Equations 18 and 20 can be rearranged as follows:

$$G_1 = \frac{2}{\mathbf{e}_o^2} E \quad (21)$$

$$G_2 = \frac{\Delta E}{\rho e_o^2} \quad (22)$$

We can now write

$$\frac{G_2}{G_1} = \frac{\Delta E}{2\rho E} = \tan \mathbf{d} \quad (23)$$

The loss factor,  $\tan \delta$ , has a peak between the glassy and rubbery states of the amorphous phase of the polymer as temperature is increased through the viscoelastic range of the polymer. The temperature at which the peak occurs is commonly cited as the Glass Transition temperature,  $T_g$ , of the material. However, in the case of semicrystalline polymers the crystalline phase of the polymer will affect the relaxation profile of the polymer and can in turn make the  $T_g$  more difficult to identify.

## 1.6 Bend-rupture

The end-loaded bend-rupture (bend-rupture) method [13] was developed to study the time dependent behavior of polymer matrix composites. The method and fixture were developed to emphasize the contribution of changes in matrix properties to the behavior of unidirectional composites loaded in the fiber direction. This method has distinct advantages over other methods such as tensile stress rupture and three and four point bending rupture methods. The following section discusses the design and fabrication of an end-loaded bending fixture. A short analysis is presented which relates strain level to end-to-end distance eliminating the need for strain gauges.

Intuitively, even though the mechanical behavior of the composite material in the fiber direction is “fiber-controlled”, the presence of a viscoelastic matrix should contribute to the global behavior of the composite. This contribution is magnified in the case of long term exposure to elevated temperatures and environment. Exposure can degrade the performance of the matrix as a load carrying and constraining constituent because in carbon

fiber composites time and environment, for the most part, affect the matrix. Such effects are difficult to quantify from tensile rupture tests of unidirectional specimens. Traditionally, off-axis laminates are tested in tension to obtain the time dependent contribution of the matrix. This is not always possible, as in the case of the current study where the material of interest is a unidirectional pultruded composite tape. Another drawback to tensile rupture tests is that they require a load frame and only one specimen at a time can be tested per load frame. Consequently, many load frames must be occupied for long periods of time in order to obtain a statistically valid data set.

A bend loading condition provides a situation where the matrix behavior contributes to the behavior of the composite system as a whole. Therefore, the time dependent changes of mechanical properties of the matrix should relate to a time dependent behavior of the system. The ASTM Standards provide bending test methods for many materials, but generally not for unidirectional PMC's in the geometry of interest. There exists considerable literature on bending as the loading condition for metals. A large variety of specimen geometry and loading configurations have been described for these materials [14]. These include three-point, four-point, cantilevered and two-point end-loaded bending conditions. Particular to the present paper, Fukuda et al [15, 16] have used end-loaded bending with increasing end displacement to determine the strength and stiffness of thin composite laminates.

Initially, three-point and four-point bending were studied as possible bending conditions. There are several drawbacks to these methods. Three-point and four-point bending conditions are difficult to obtain for a large number of specimens in a confined space. Moreover, the need for a fixture enabling the bending of the specimens within a wide range of strain levels requires the apparatus be quite complicated. These methods also introduce stress concentrations at the loading noses, and can induce matrix cracking and premature failure of the specimen while masking the bulk behavior to be studied.

An end-loaded bending condition was chosen because of the simplicity of the required fixture. The end-loaded bending condition requires only the application of a single axial force, with the test specimen making contact with the fixture at only two points. This avoids the fixture causing the failure, as is often the case for three and four point bending. End-loaded bending also constrains the specimen very little, allowing the specimen to redistribute stress and strain freely. A large range of strains is obtainable by simply adjusting the length between the loaded ends of the specimen. The end-loaded bending condition is shown in Figure 1-3.



**Figure 1-3 End-loaded bending condition**

### **1.6.1 Bend-Rupture Fixture**

A fixture was developed to employ this bending condition. Preliminary bending experiments, on the material of interest, showed that a relatively small load, on the order of 10 pounds, was required to constrain each specimen. As a consequence, the fixture did not need to be overly robust to support these loads. A simple tension support member with a means to constrain the loaded ends was all that was needed. Intuitively, the experiments conducted at low strain levels were expected to be long-term experiments. Also, the tests were to take place at elevated temperatures. Consequently the fixture had to be compact and able to withstand hostile environments.

Such a fixture was fabricated of 0.04-inch 304 18-8 cold rolled and annealed stainless steel because of its availability, dimensional stability at temperature, and resistance to corrosion.

An adjustable fixture able to load only one specimen, Figure 1-4 a, was fabricated by hand using a bench vice and hole punch. This fixture, with a loaded specimen, is shown in Figure 1-1 b. A one piece fixed-length fixture able to load as many as 15 specimens at the same strain level, shown in Figure 1-4 c, was built for long term rupture tests. This fixture has a longer upright at one end so that specimens can be loaded by initiating a small bend in the specimen and then sliding one end down the longer upright. In this way, intended strain levels are not exceeded when loading specimens and a load frame is not needed.

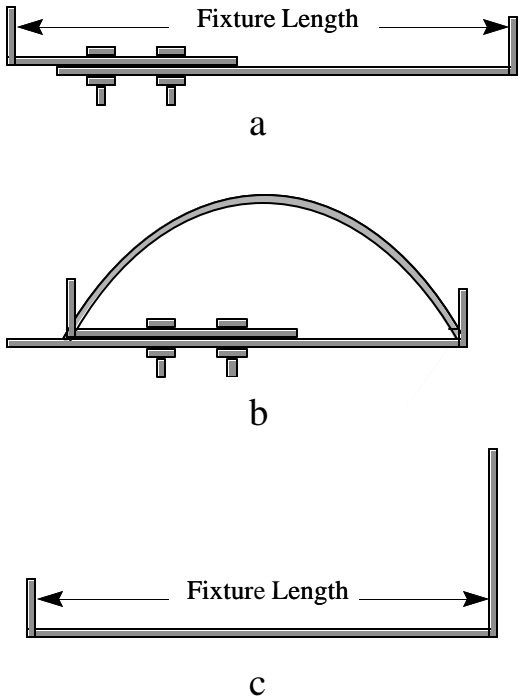


**Figure 1-4 End-loaded bend rupture fixture**

### 1.6.2 Specimen Geometry

This method is most effective for specimens that are thin and require large mid-span deflections to obtain the desired strain levels. For materials with similar mechanical properties, thicker specimens are required to be longer and longer fixtures are required to accurately obtain desired strain levels. In all cases, care should be taken to align the specimen so that both loaded ends of the specimen are parallel to the loading surface of the fixture. This will avoid shear loading that can cause longitudinal splitting of the specimen.

### 1.6.3 Analysis

The end-loaded bending condition is identical to the pinned-pinned post-buckling condition of a beam addressed by the elastica analysis. This condition is shown in Figure 1-5.

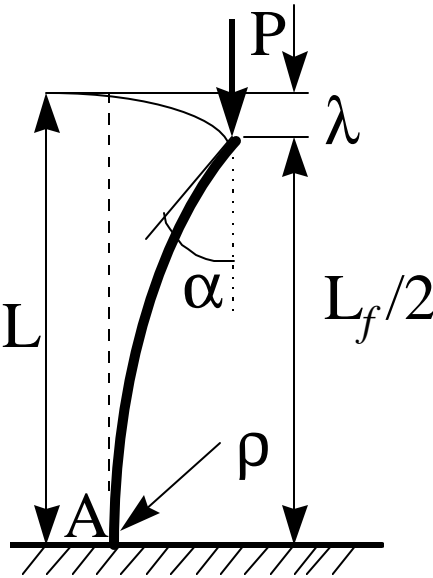


Figure 1-5 Pinned-pinned post-buckling loading condition

Through this analysis the maximum strain can be related to the end-to-end length. From work done by Timoshenko [17] and Fukuda [15, 16], applying the elastica solution and classical strength of materials, we can relate fixture length,  $L_f$  to maximum surface strain,  $\epsilon_m$ . The relationship may be obtained as follows.

Assuming that the material stiffness is the same in both tension and compression,  $E_t = E_c$ , the maximum strain is given by

$$\mathbf{e}_m = \frac{t}{2\mathbf{r}} \quad (24)$$

where  $t$  is the thickness of the specimen,  $\mathbf{r}$  is the radius of curvature of the loaded specimen at the point of maximum curvature, A. The radius of curvature is given by

$$\mathbf{r} = \frac{1}{2pK(p)} L \quad (25)$$

where

$$p = \sin \frac{\alpha}{2} \quad (26)$$

$\alpha$  is the end rotation and

$$K(p) = \int_0^{\frac{\pi}{2}} \frac{1}{\sqrt{1-p^2 \sin^2 \mathbf{f}}} d\mathbf{f} \quad (27)$$

is the first perfect elliptic integral.  $L$  is the half-length of the specimen. End displacement can be determined by

$$\mathbf{I} = \left( 2 - 2 \frac{E(p)}{K(p)} \right) L \quad (28)$$

where

$$E(p) = \int_0^{\frac{p}{2}} \sqrt{1 - (p^2 \sin^2 f)} df \quad (29)$$

is the second perfect elliptic integral. From the previous relationships, a parametric relationship between the end displacement, and the radius of curvature can be determined as a function of end rotation  $\alpha$ . The end-to-end distance is given by  $L_f = 2(L - \lambda)$ . Now strain and end-to-end distance can be related. This analysis includes a correction of an error found in Fukuda [15].

Initial experiments were conducted to validate this analysis. Specimens were strain gauged at the mid-span and loaded into the single specimen adjustable fixture. The end-to-end distance was measured and the strain level was obtained from the strain gauge. Figure 1-6 represents fixture length, in this case, as a function of normalized maximum strain. The normalized maximum strain is the mid-span surface strain normalized by the room temperature tensile strain at failure. Included in Figure 1-6 are the experimental data obtained with the adjustable fixture.

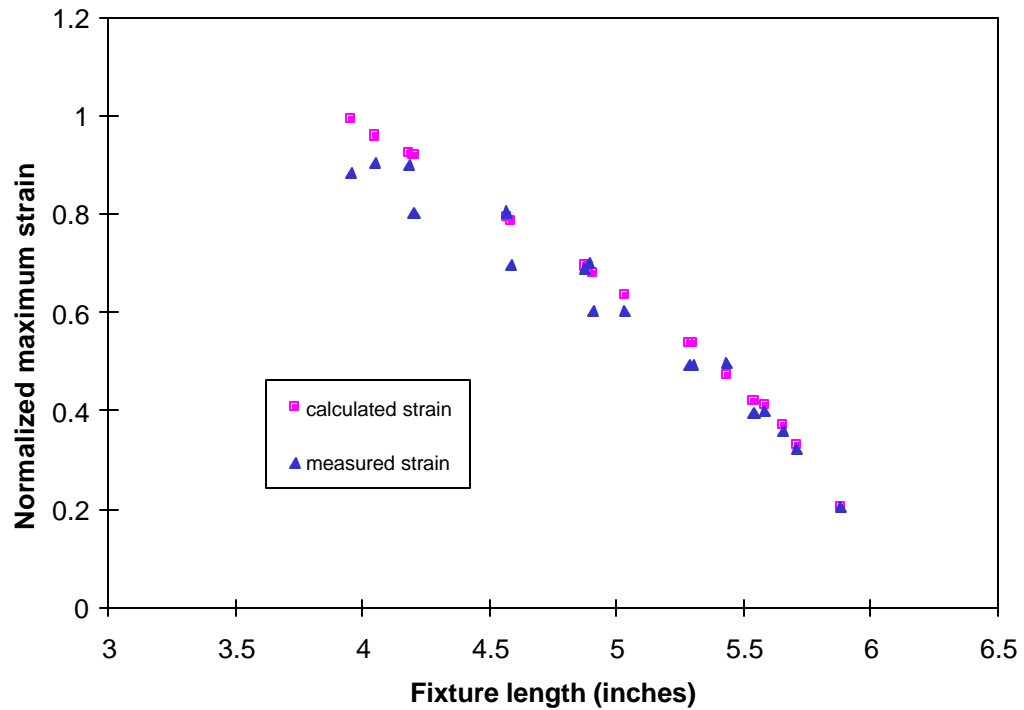


**Figure 1-6 Normalized strain vs. fixture length**

There is a good correlation between experimental and theoretical values; the average error is about 6%. The calculated strains seem to provide an upper bound to the measured values. The error can largely be explained by the fact that the 0.25 inch strain gages used averaged the strain around the point of maximum strain and do not report the actual maximum strain. Also contributing to the error is the fact that the previous equations assume a constant and uniform bending modulus. It is possible that the compressive and tensile stress-strain response differ slightly so that the  $\epsilon=0$  at geometric centerline assumption is no longer exact. From the behavior of the data and the small error compared to theoretical expectations, it is concluded that these fixtures ensure the correct loading condition and provide reproducible

data. With such good correlation, strain gauges need not be applied to specimens with constant and known thickness to ensure that specific strain levels are accurately reached.

This method is simple to implement and sensitive to subtle differences in matrix material. Furthermore this method does not require the use of strain gauges to obtain a desired strain level. These data form a basis, along with determination of the failure mode, for development of analytical models for bending behavior of unidirectional PMC's, enabling service life predictions for systems undergoing out-of-plane deformations at elevated temperature. The bend-rupture method has been used by several researchers [18, 19], to study the long-term response in bending to elevated temperatures both under static and fatigue loading. Also a methodology [20] has been developed to predict tensile rupture lives from bend-rupture data through use of micro-mechanics.

## **1.7 Composite Life Prediction**

Life prediction of composite materials subjected to combined loading is often a key aspect of design. Combined loads may be comprised of quasi-static mechanical loads (tension, compression, shear, etc.), mechanical fatigue, elevated temperatures, thermal cycling and chemical degradation. It is usually not possible to include all of these factors and their variations in a single test. Therefore it is necessary to have an analytical method for combining the applicable conditions to predict the life of composites.

In order to use this material for this application, the service life prediction must include the effects of fatigue and elevated temperatures up to 90°C. The service life model for the material under consideration was constructed using the methodology proposed by Reifsnider et al [21]. This methodology has been used for a variety of material systems in many service environments and has been integrated into a performance simulation code, MRLife, developed by the Materials Response Group at Virginia Tech [22, 23, 24]. This

methodology uses experimental data and analytical tools to predict the long-term behavior of a composite. The methodology's adaptation to the present work [25] is detailed in Chapter 5.

## **1.8 Summary: Chapter 1**

Chapter 1 introduced the context in which the present work was undertaken along with foundation that this work extends. The object of this work is presented and the motivation to use a composite material in a non-bonded flexible riser for use in the offshore oil industry is put forth. The requirements for such a material is detailed. Strength analysis and modeling methods are presented. The effect of matrix crystallinity on composite mechanical properties is briefly discussed. A standard method for investigating matrix behavior at elevated temperatures is review and a new method is developed. A remaining strength life prediction methodology is recalled as support for later work. With these topics in mind, the following chapters are outlined.

Chapter 2 discusses the experimental methods employed to gather the experimental data in the present work

Chapter 3 introduces the specific composite in detail, presents preliminary data, and illuminates differences in mechanical properties due to processing parameters and describes their cause.

Chapter 4 presents experimentally determined static strength, fatigue behavior at room and elevated temperatures, and tensile rupture data.

Chapter 5 develops and validates a remaining strength approach for life prediction for the case of combined fatigue and rupture loading.

Chapter 6 summarizes the key findings presented in the present work and draws conclusions from these findings. Future areas of work are also listed.

## Chapter 2

### 2 EXPERIMENTAL METHODS

The initial interest in the present material was its response to the loading and environmental conditions associated with use as a helically wound tension member in a flexible riser. These conditions consist of static loads, cyclic loads, and exposure to elevated temperatures due to service conditions, as well as confinement to a bent geometry during storage as the composite awaits the riser manufacturing process and as the completed riser awaits deployment. The following experimental methods and procedures were employed in the investigation the material's response to the flexible riser environment.

- Quasi-static tensile tests
- Tensile rupture tests
- Tension-tension fatigue tests
- End-loaded bend rupture tests
- Dynamical Mechanical Analysis (DMA)
- Environmental aging

The following section describes these test methods and procedures.

#### 2.1 Quasi-Static Tensile Test

Quasi-static tensile tests were conducted within the ASTM D 3039 standard [26]. All Quasi-static test results reported in the present work were conducted in Material Testing Systems (MTS) servo-hydraulic load frames. A typical quasi-static tensile test specimen, tabbing materials and tabbed specimen are shown in Figure 2-1. Specimens used for all testing (except where stated otherwise) were 6 inches in total length with a 3-inch test section. The cross section of the composite, 0.5 inches by 0.04 inches, was fixed by the

pulltrusion manufacturing process. The length, however, was not constrained as the composite tape was delivered in continuous lengths of up to 1500 feet. The specimens were cut using a water-cooled tile-cutting saw with a diamond-impregnated blade. Quasi-static specimens were tabbed to improve gripping in the load frame and reduce damage caused by the grip wedges.

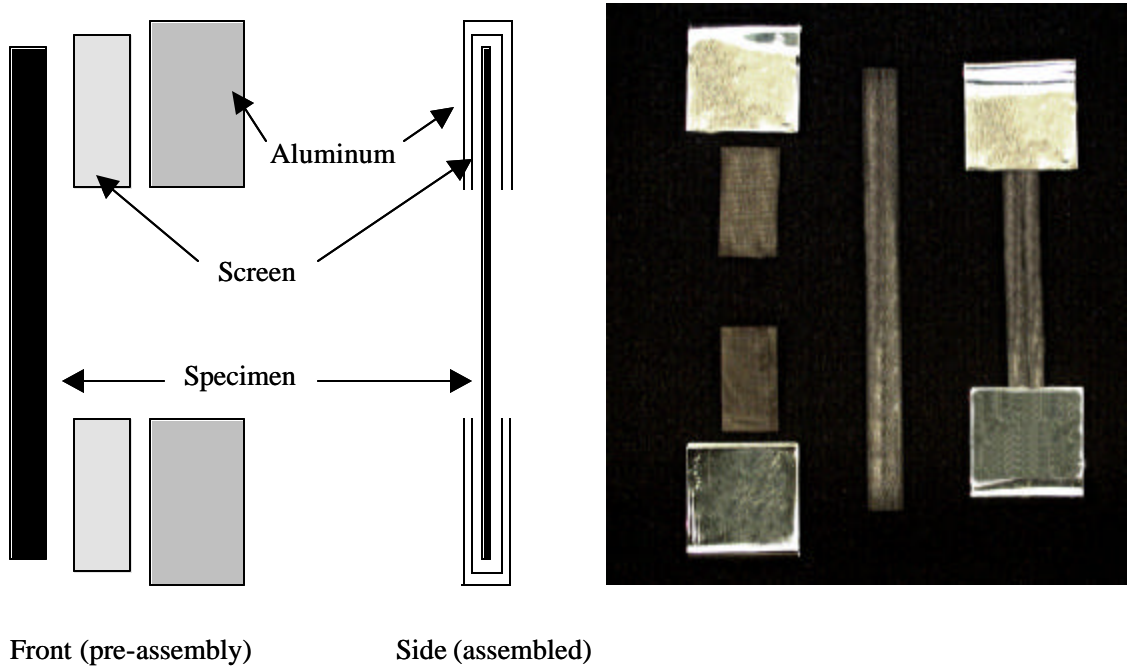


**Figure 2-1 Typical tensile specimen and tabbing**

The tabbing materials used consisted of 100-count (100 wires per linear inch) stainless steel screen and 1000 series aluminum sheet that was 0.02 inches thick. The screen was cut into 0.75 by 3.0 inch rectangles using a utility knife. The aluminum sheet was delivered as a 1.5 inch wide tape and was cut to a 3.25 inch length with a paper cutter. The screen was then folded in half around the end of the specimen and the aluminum also folded in half was placed around the end to the specimen as shown in Figure 2-1.

Quasi-static tests were performed in load control at a specified constant load rate. The load-time trace for a quasi-static tensile test is shown in Figure 2-2. A typical stress-strain plot, Figure 2-3, for the quasi-static test produces a slightly concave-up trace as the material stiffens slightly with increased load.

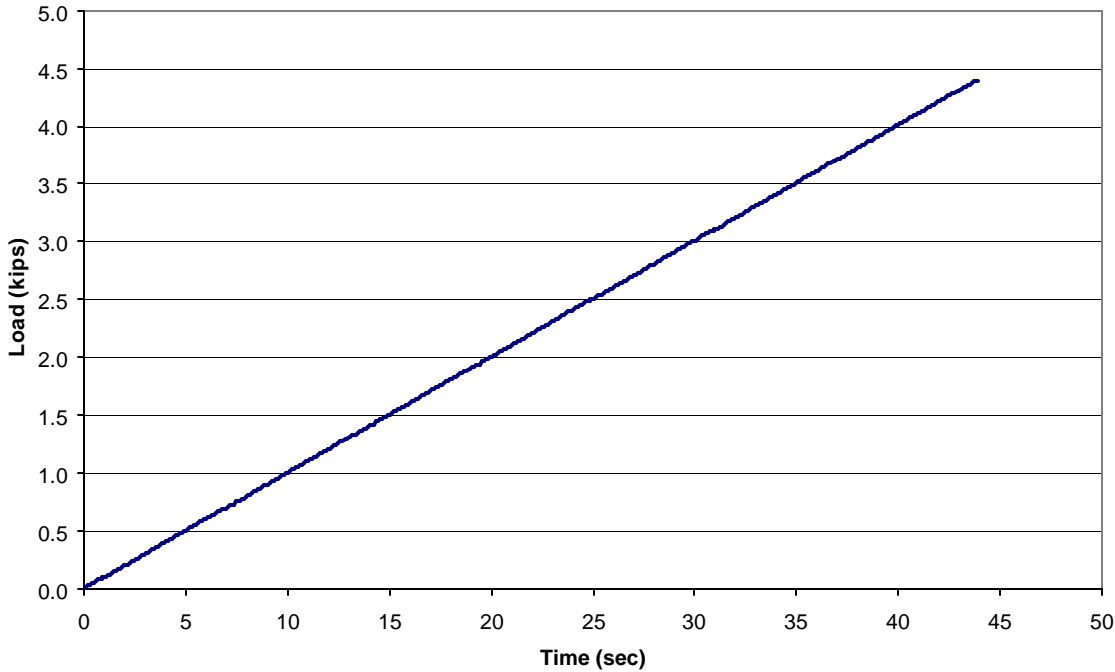


**Figure 2-2 Typical quasi-static tensile test load-time trace**

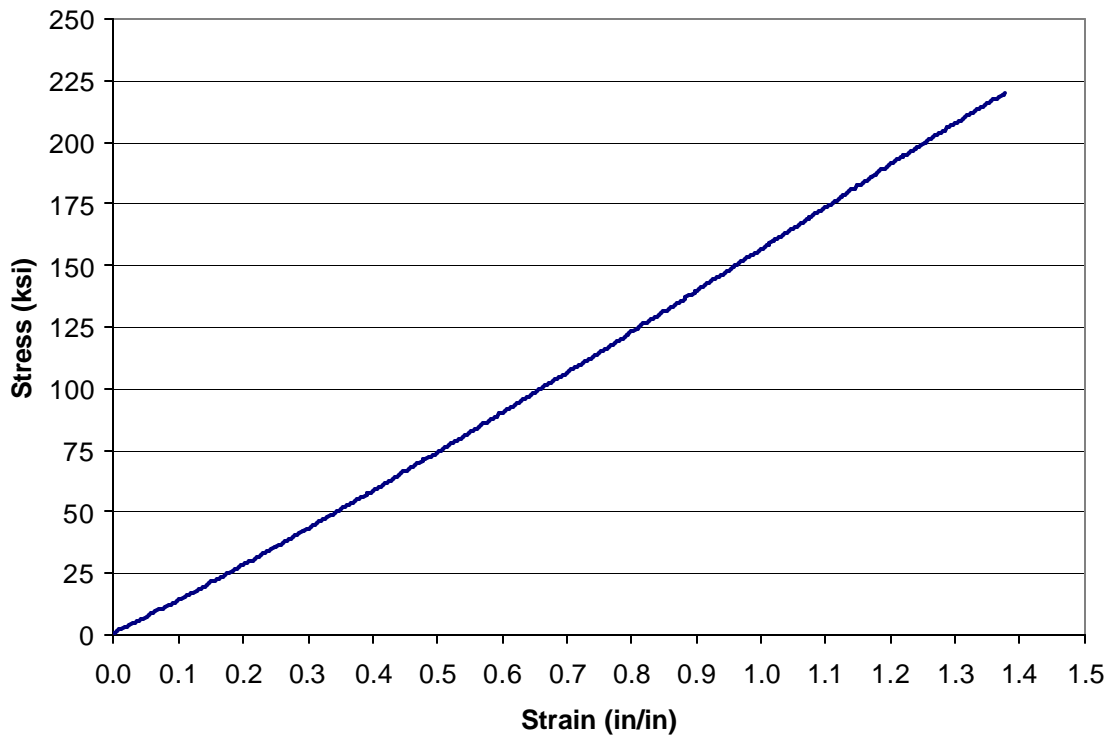


**Figure 2-3 Typical quasi-static tensile test stress-strain curve**

This trace is very close to linear and therefore was considered so in determining tensile modulus. The secant modulus, measured as the slope of the line between the origin and point of failure of the stress-strain plot, was reported as the tensile modulus. This is a deviation from the ASTM standard, which specifies that a cord modulus between 0.10 % and 0.30 % strain should be reported as the stiffness of the composite. The standard was deviated from as a matter of convenience in reducing data. The results obtained from the two methods are comparable.

Strain was measured using a strain gage during initial tests and an extensometer for later tests. Because of the linear stress-strain to failure behavior of the material under study, strength results are reported as the stress at failure.

All test results reported for a single data set were obtained from tests having identical loading rates. However, for loading rates from 50 pounds/sec to 2000 pounds/sec there is no observed effect on the strength measured, as illustrated in Figure 2-4. These loading rates correspond to strain rates from  $1.7 \times 10^{-4}$  1/sec to  $6.7 \times 10^{-3}$  1/sec.

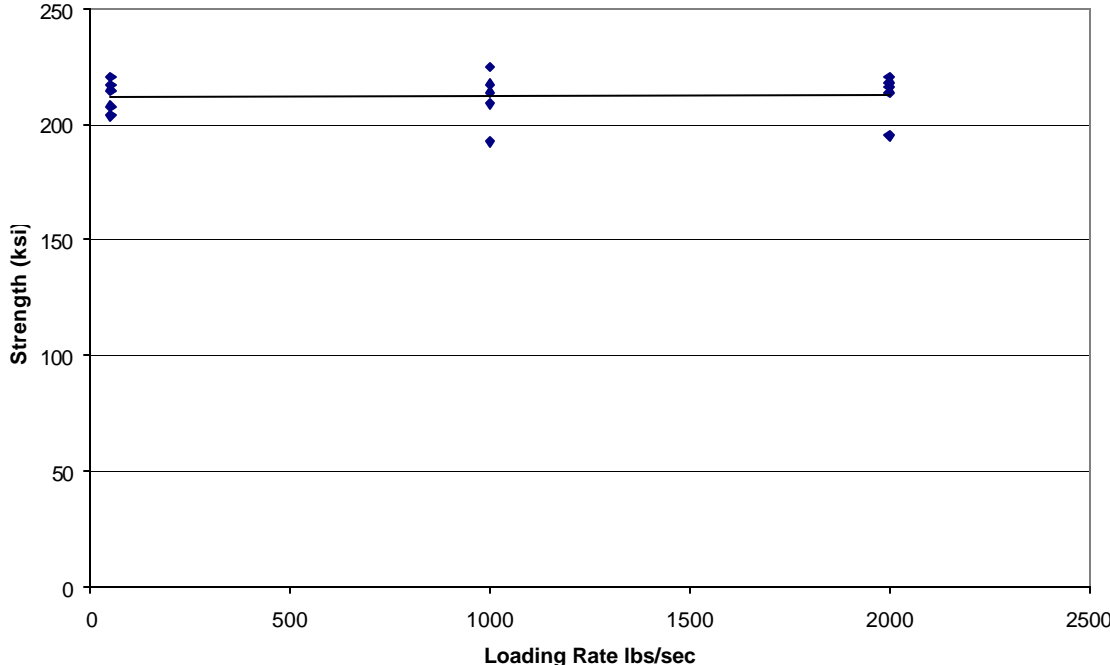


**Figure 2-4 Measured quasi-static tensile strength versus loading rate**

A hydraulic grip line pressure of 800 psi, producing a clamping force of approximately 12,000 pounds, was used for all quasi-static tensile, tensile-rupture, and tension-tension fatigue tests. During the initial stages of characterizing the material of interest, the measured

strength values were found to be sensitive to grip pressure; higher pressures produced lower strength results. Also, lower grip pressures led to slipping of the specimen in the grip wedges. A grip pressure of 800 psi provided very reliable gripping, without slipping, and consistent strength results.

Quasi-static tensile tests were also run at elevated temperatures. An oven (Figure 2-5) constructed by Mr. McCord of the Materials Response Group was employed to obtain the desired testing temperature. This oven consisted of a steel sheet metal box connected to an industrial handheld heat gun via a 3-inch flexible aluminum duct. Temperature control was achieved with a PID controller. The control loop consisted of the PID controller connected to the heating elements of the heat gun and thermocouple placed in the oven box to provide temperature feedback. The tabbing, grip pressure and loading rate were the same as for the ambient quasi-static tensile tests.



**Figure 2-5 MTS load frame with box heater**

## 2.2 Tensile Rupture Test

Tensile Rupture tests were also performed on a Material Testing Systems (MTS) servo-hydraulic load frame. This frame was equipped with an environmental chamber, shown in Figure 2-6, and controller, manufactured by Russells Technical Products, capable of creating both elevated and sub-ambient temperatures and humidities. Heating was accomplished by electric resistive heating elements and cooling by externally supplied liquid nitrogen. Grip extensions positioned the entire grip assembly within the environmental chamber so that when tests are run the specimen including the end-tabbed sections were in thermal equilibrium at the test temperature.

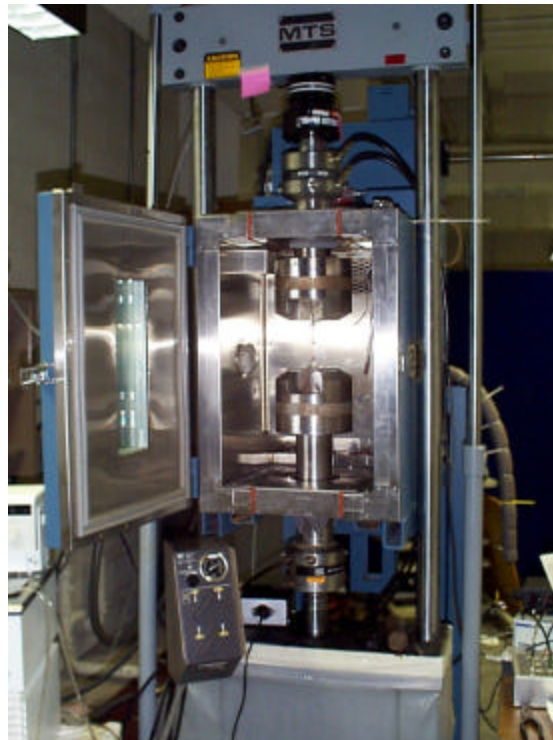


**Figure 2-6 Load frame and environmental chamber**

The load profile for the tensile rupture tests consisted of an initial ramp and a subsequent hold at the desired load until failure. This profile is shown in Figure 2-7.

The specimens, tabbing method, and grip pressure used in the tensile rupture tests were identical to those used in the quasi-static tensile tests. Results from the tensile rupture tests are reported as time to failure at a given temperature for the applied hold load. Strain-time traces could also be obtained from these tests when an extensometer was used to measure strain.

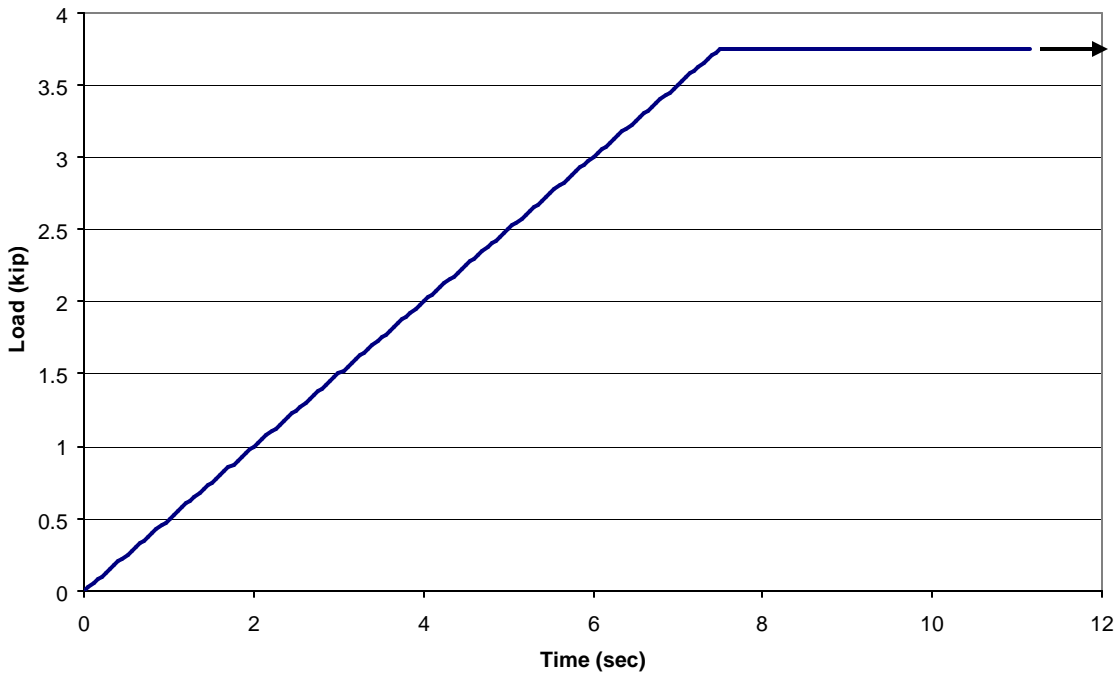


**Figure 2-7 Typical tensile rupture test load-time trace**

### 2.3 Tension-Tension Fatigue Test

Tension-tension fatigue tests were conducted within the ASTM D 3479 standard [27]. These tests were performed on the same Material Testing Systems (MTS) servo-hydraulic load frame as the quasi-static tensile tests. The load history for the tension-tension fatigue tests consisted of a sinusoidal load profile at a frequency of 10 Hz that oscillated between a maximum load and ten percent of that maximum load ( $R= 0.1$ ). The load profile, shown in Figure 2-8, was entirely in tension. Because of the limitation on material cross-section imposed by the pultrusion process, specimens were not acceptable for tension-compression testing at meaningful lengths. Specimens, tabbing method, and grip pressure used in the tension-tension fatigue tests at room temperature were identical to those used in the quasi-static tensile tests.

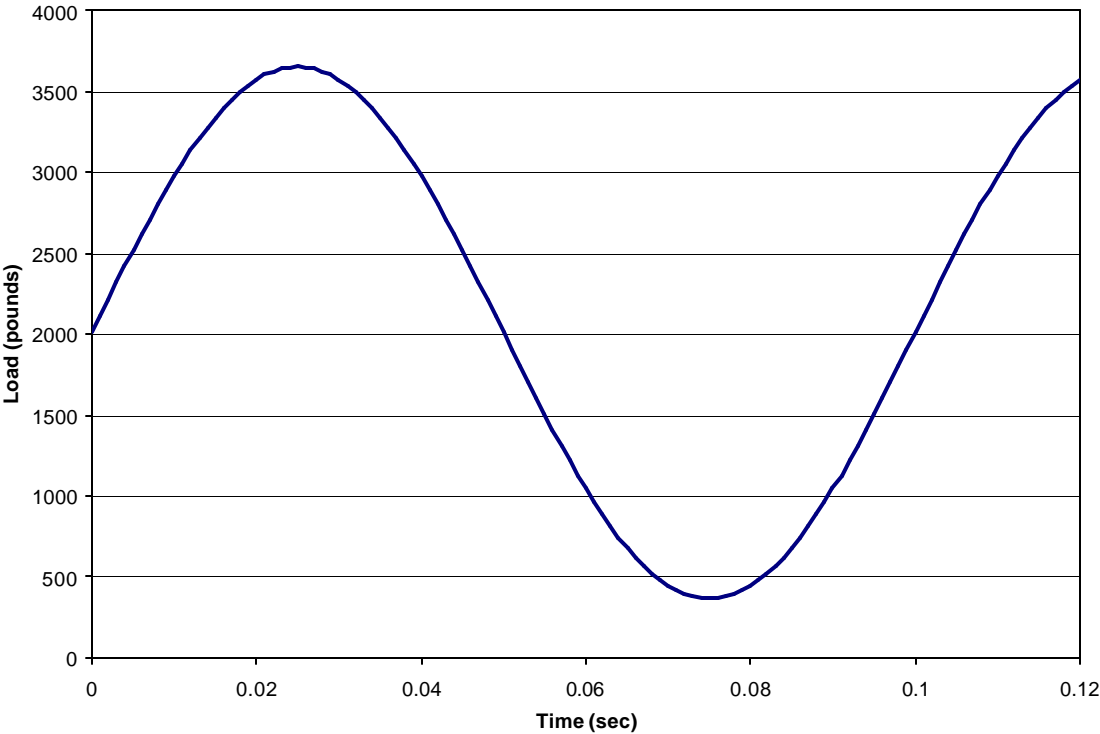


Figure 2-8 Typical tension-tension fatigue test load-time trace

Tension-tension fatigue tests were also conducted at elevated temperatures. These tests utilized the same specimen geometry, tabbing method and grip pressure as the quasi-static tensile test specimens. The oven used was also of the same type used for the elevated temperature quasi-static tensile tests. Results for all tension-tension fatigue tests are reported as cycles to failure at a given maximum stress, R-ratio, and test temperature.

## **2.4 End-Loaded Bend Rupture Test**

As mention earlier, much of the present material characterization work was motivated by the material's use in flexible risers. The bend-rupture test method [28] was developed to examine the long-term behavior of the composite in a bent geometry while exposed to elevated temperatures and aggressive environments. A brief analysis the specimen loading and a description of the test method development is given in Chapter 1.

### **2.4.1 End-Loaded Bend Rupture Fixture**

An adjustable prototype fixture was used to obtain the bend-rupture data in this study. This fixture, with and without a loaded specimen, is shown in Figure 2-9. A Fisher Scientific Isotemp vacuum oven was used for the end-loaded bend rupture tests. This oven's large thermal mass and glass window made it ideal for these tests. The tests were preformed by placing the fixture with loaded specimen into the oven, which was preheated to the desired test temperature. A stopwatch was used to measure the time between the specimen being placed in the oven and the time the specimen failed. The results from the bend rupture tests are reported as time to failure at a given normalized maximum strain and testing temperature. The normalized maximum strain is the mid-span surface strain normalized by the room temperature tensile strain at failure.

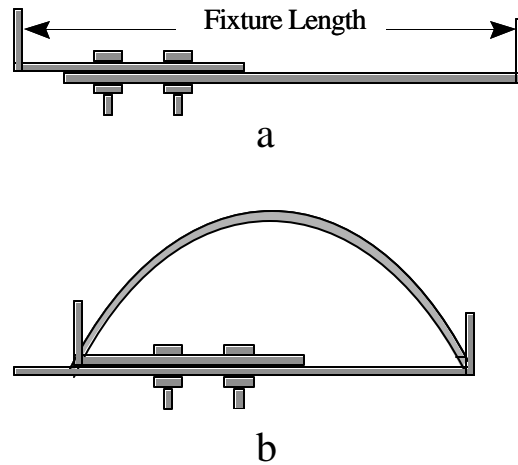


**Figure 2-9 End-loaded bend rupture fixture**

## **2.5 Dynamic Mechanical Analysis (DMA)**

Dynamic Mechanical Analysis was used to determine the relaxation profile of the carbon/PPS composite. The DMA was performed at a fixed frequency of 1 Hz and a maximum displacement of 0.006 inches and the temperature was varied from 35° to 175° C at a rate of 1° C/min for all specimens tested. The specimens used in the DMA were 2 x 0.5 x .04 inches in dimension. The  $\tan \delta$  curve gives the relaxation profile of the material. These tests were performed on a Thermal Analysis Instruments 983 DMA that employs a cantilever bending geometry to displace the specimen. Figure 2-10 shows a typical DMA plot. A brief description of the viscoelastic behavior measured by the DMA is given in Chapter 1.

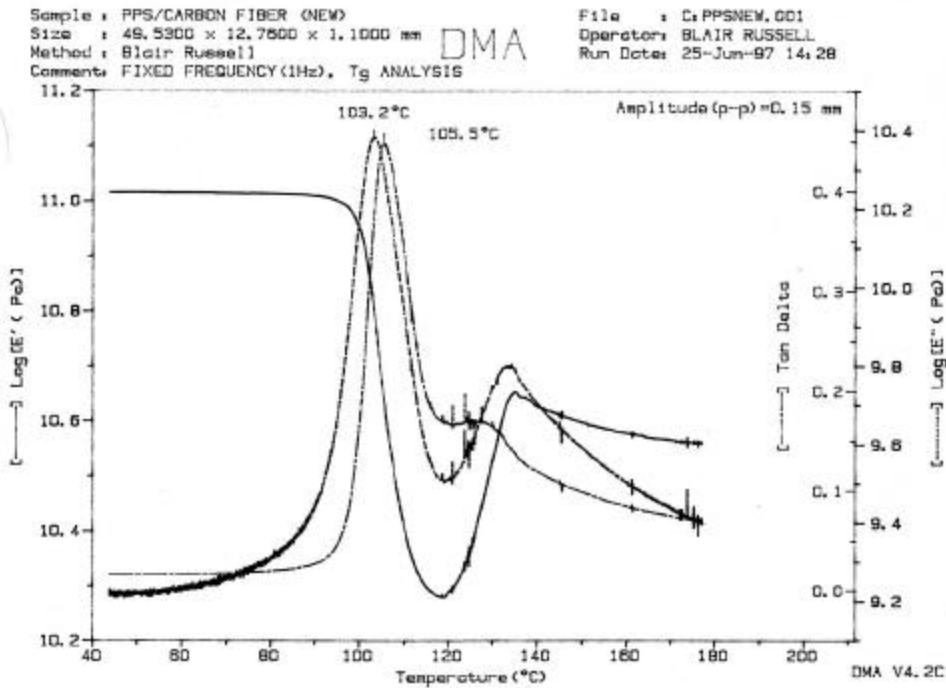


**Figure 2-10 Typical DMA plot**

## 2.6 Environmental Aging

Tests were performed on the material after exposure to elevated temperatures in air and seawater. Aging in air was accomplished by placing the specimens on wire racks in a vacuum oven and held at a constant temperature for the duration of aging. In order to age material in seawater at elevated temperatures, specimens were arranged in racks fabricated of G10 glass/epoxy laminate, and then placed in a 10.5 quart glass box filled with seawater. The glass box was constructed of six 0.25-inch thick glass plates sealed with silicone. The seal between the top plate and the four sides was cut with a razor blade so the top could be removed to allow access to the specimens and pressure relief. The seawater was heated by placing the glass box on a wire rack in the vacuum oven and allowing the temperature of the

seawater to come to equilibrium with the oven. Because of the large thermal mass of the oven, it was ideal for heating the seawater and maintaining a constant temperature over long periods of time. Seawater was simulated using Instant Ocean. This product, manufactured by Aquarium Systems USA & France, contains sodium chloride and other trace elements in concentrations (when mixed as directed) typical of the ocean environment. The product is intended to produce simulated seawater for saltwater aquariums.

Aged material was tested using the same procedures as unaged material. The aging of material is reported as the aging duration at a given temperature in a given environment (i.e. air or seawater).

## **2.7 Summary: Chapter 2**

Chapter 2 describes the experimental test methods and procedures employed in the present study. Table 2-1 summarizes these methods and describes the manner in which the results are reported.

**Table 2-1 Tests methods and procedures**

<b>Method or Procedure</b>	<b>Loading Method</b>	<b>Specimen Dimension (L x W x T)/ gage length inches</b>	<b>Results</b>	<b>Test Parameters</b>
Quasi-static tensile test	Tension, Ramp to failure	(6.0 x 0.5 x .04)/ 3.0	Strength (ksi) Modulus (Msi) Strain @ failure (%)	Load rate (lbs/sec) Grip line pressure (psi) Test temperature (°C)
Tensile rupture test	Tension, Ramp and hold to failure	(6.0 x 0.5 x .04)/ 3.0	Time to failure (sec)	Load rate (lbs/sec) Hold stress (normalized) Grip line pressure (psi) Test temperature (°C)
Tension-tension fatigue test	Cyclic Tension, Sinusoidal cycled to failure	(6.0 x 0.5 x .04)/ 3.0	Cycles to failure(cycles)	Load frequency (Hz) R-Ratio Max stress (normalized) Grip line pressure (psi) Test temperature (°C)
End-loaded bend rupture test	Post buckled bending, Constant end-displacement	(6.0 x 0.5 x .04)/ 3.0	Time to failure (sec)	Max Strain (normalized) Test temperature
Dynamical Mechanical Analysis (DMA)	Cantilever bending	(2.0 x 0.5 x .04)/ 1.5	Tg Stiffness modulus Loss modulus Tangent delta	Frequency (Hz) Heating Rate (°C/min) Max displacement
Environmental aging	Not loaded	As need for subsequent tests	NA	Duration (days) Temperature (°C) Environment (air or seawater)

## Chapter 3

### 3 THE EFFECTS OF TEMPERATURE AND PROCESSING HISTORY ON COMPOSITE MECHANICAL PROPERTIES

During the initial investigation of the carbon fiber/PPS composite, several inconsistencies in the material properties were observed between two deliveries of material. Also of interest, quasi-static tensile tests of material aged at elevated temperatures yielded unexpected results. The present chapter presents the initial quasi-static tensile and bend-rupture test results, subsequent DMA results, and an investigation of the effects of manufacturing processing parameters on the tensile properties and bend-rupture behavior of the composite.

#### 3.1 Composite and its Constituents

Baycomp of Burlington, Ontario, Canada, manufactured the material under study. The composite is a carbon fiber/polyphenylene sulfide (PPS) pultruded composite tape with a 0.5 x.04 inch cross section. The composite tape consists of approximately 50% by weight or 40% by volume carbon fiber with the remainder made up PPS polymer.

##### 3.1.1 Fiber

The carbon fibers in the composite under study are Grafil 34-700 standard modulus carbon fibers. The composite contains 12, 12k (12,000 filament) tows of this fiber. Typical properties [29] for Grafil 34-700 carbon fibers are given in Table 3-1. The mechanical properties of the fibers are taken to be constant in the temperature range under consideration.

**Table 3-1 Typical properties of Grafil 34-700 carbon fiber [29]**

Number of Filament	Strength* ksi	Modulus* msi	Density lb/in <sup>3</sup>	Yield yds/lb	X-sectional area in <sup>2</sup>	Elongation %	Filament Diameter $\mu\text{m}$
12000	650	34	0.065	620	6.89x10 <sup>-4</sup>	1.9	7

\* Impregnated Strand Test-SACMA Methodology

### 3.1.2 Matrix

The matrix material of the composite is polyphenylene sulfide (PPS), a semi-crystalline thermoplastic. The PPS in the material of interest is manufactured by Phillips Petroleum Company and marketed under the trade name Ryton. PPS is an attractive polymer because of its thermal stability and chemical resistance. Typical room temperature mechanical properties of PPS [30] are given in Table 3-2.

**Table 3-2 Typical room temperature (25°C) mechanical properties of PPS**

Tensile Strength (ksi)	Elongation (%)	Flexural Strength (ksi)	Flexural Modulus (ksi)
12.5	3.0	21.0	600

Of particular importance in the present study is the viscoelastic nature of the matrix material of the composite. As reviewed in Chapter 1, PPS is viscoelastic, i.e., can exhibit behavior that ranges from that of an elastic solid to that of a viscous fluid with a strong dependence on temperature and time. Typical physical properties of PPS are given in Table 3-3. The mechanical properties of the composite can be correlated to the relaxation profile. Also of note is that the stiffness of the polymer is dependent on the degree of crystallinity and can also be affected by the presence of fibers that inhibit the mobility of the polymer.

**Table 3-3 Typical room temperature physical properties of PPS [30]**

Glass Transition Temperature	Melt Temperature $T_m$ (°C)	Max Crystallization Temperature from melt $T_c$ (°C)	Max Crystallization Temperature from glassy state $T_c$ (°C)	Specific Gravity
85	285	230	130	1.35

### 3.1.3 Constructing the Composite

The PPS matrix and fibers are combined to form a composite tape through a pultrusion process. A schematic of the manufacturing process is given as Figure 3-1. Fiber tows are introduced into the manufacturing process from spools. These tows are then separated and aligned as they enter the next stage of the process. The next step involves a proprietary method of impregnating the fiber tows with powdered PPS. It is suspected that this process involves using an electrostatic charge to attract the powder to the fibers. Of particular interest to the present work are the heating, consolidation, and cooling segments of the process. After the PPS is deposited on the fibers, it is drawn into the heated end of the die. The temperature of the fiber/matrix is brought to above the melt temperature,  $T_m$ , of PPS and the tape continues into the consolidation part of the die where it is forced into its final cross sectional shape and size, and then cooled. The composite may then go through an additional cooling stage before it reaches the puller and runs through a composite tape accumulator then on to a take-up reel. It is important that the composite temperature be well below the  $T_g$  of the matrix before it reaches the puller, accumulator, and take-up reel to prevent permanent deformation of the composite tape.

In the following discussion all composite runs had the same constituents; differences in runs are due to processing parameters only. The processing parameters of interest are the pull-rate, method of cooling and exit temperature. These parameters determine the cooling rate of the composite.

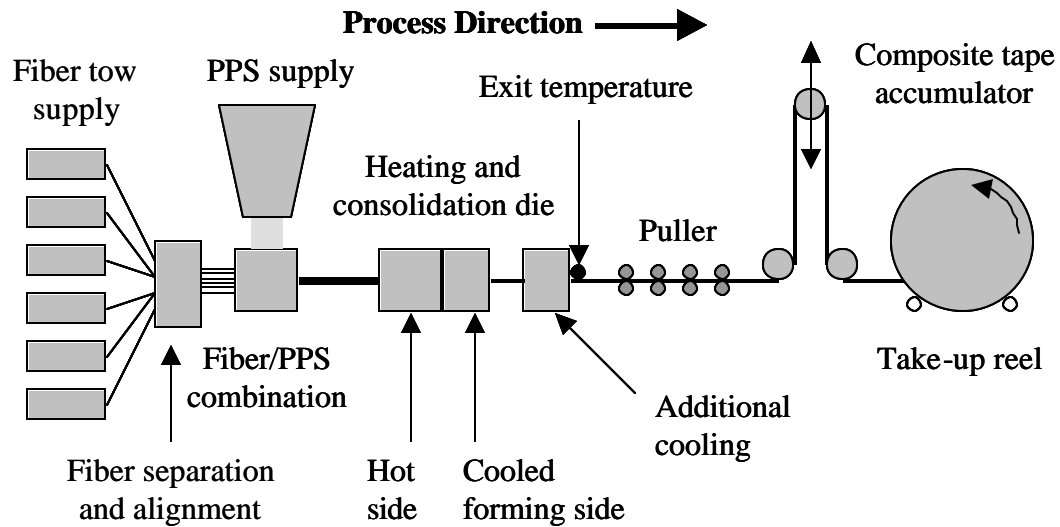


**Figure 3-1 Schematic of composite tape pultrusion manufacturing process**

### **3.2 Material From Run 1 and Run 2**

Material from two manufacturing runs was received from the composite manufacturer and tested. The first material received, Run 1, was from a trial run where only 30 pounds of composite were produced. The second material, Run 2, was from a full-scale production run where 5000 pounds of composite were produced. These materials are reported, by the manufacturer, to have identical constituents, however the processing information was not preserved and is not available for these runs.

#### **3.2.1 Preliminary Tests Results**

Quasi-static tension tests, fiber volume fraction measurements as well as bend rupture tests were performed on material from these runs. The results from the Quasi-static tests show that there was little difference in strength (5.4%) or modulus (2.8%) between the materials from the two runs. These results along with the fiber volume fraction measurements are

presented in Table 3-4. The fiber volume fraction,  $v_f$ , measurements were made following the Archimedes principle. Because the results of this method are susceptible to errors in the measurement of specimen volume due to surface roughness and, in this case, because of the limited number of replicates, the accuracy of these results should be viewed accordingly. The manufacturing technique makes differences in  $v_f$  unlikely if the cross section remains the same. In addition, the measured strength and stiffness values counter indicate the  $v_f$  measurements.

**Table 3-4 Comparison of room temperature Run 1 and Run 2 properties**

<b>Material</b>	<b>Strength (ksi)</b>	<b>Modulus (msi)</b>	<b>Fiber Volume Fraction (%)</b>
Run 1 (10 replicates)	186 ± 5.5	14.3 ± .13	44 (2 replicates)
Run 2 (10 replicates)	196 ± NA	14.7 ± NA	39 (2 replicates)

NA indicates data no longer available

### 3.2.2 Quasi-Static Strength Data

Quasi-static strength, modulus, and strain to failure measurements of Run 1 material were made by the quasi-static tensile test method. Initial strength and modulus at 23, 90 and 120 °C are presented in Table 3-5. To determine the effect of unstressed exposure to elevated temperatures, specimens were aged in air at 90 and 120 °C for 1, 10, 30, and 100 days and then tested at room temperature to evaluate residual strength. Quasi-static tensile properties are also given in Table 3-5.

**Table 3-5 Run 1 tensile properties at temperature and post aging**

	<b>Modulus Msi</b>	<b>Strength Ksi</b>	<b>Strain to Failure %</b>
Quasi-Static Tension Test Results of un-aged material			
23 °C (10 replicates)	14.3 ± .13	186 ± 5.5	1.41 ± .033
90 °C (5 replicates)	13.6 ± .26	188 ± 8.4	1.46 ± .061
120 °C (5 replicates)	13.2 ± .36	174 ± 7.8	1.37 ± .081
Quasi-Static Tension Test Results of Aged Specimens (tested at 23 °C)			
1 Day @ 90 °C (10 replicates)	14.3 ± .44	197 ± 14.4	1.41 ± .13
10 Day @ 90 °C (10 replicates)	14.2 ± .33	199 ± 8.4	1.44 ± .054
30 Day @ 90 °C (10 replicates)	14.2 ± .20	194 ± 6.7	1.46 ± .072
100 Day @ 90 °C (4 replicates)	14.3 ± .70	194 ± 11.6	1.41 ± .061
1 Day @ 120 °C (10 replicates)	14.3 ± .27	209 ± 6.3	1.55 ± .042
10 Day @ 120 °C (10 replicates)	14.0 ± .48	199 ± 12.4	1.50 ± .062
30 Day @ 120 °C (10 replicates)	14.4 ± .26	202 ± 5.4	1.47 ± .053
100 Day @ 120 °C (10 replicates)	14.5 ± .66	194 ± 5.1	1.44 ± .096

The data in Table 3-5 show that unstressed exposure to air at 90 and 120 °C up to 100 days enhances the quasi-static tensile strength of the material when compared to un-aged material. These results are counterintuitive, as prolonged exposure to elevated temperatures is generally considered detrimental to polymers. The strength of the material, under both aging conditions, is higher after exposure and the stiffness remains approximately the same in the case of 90°C aging and may show a slight increase in the case of 120°C aging. Of note, there is a monotonic decrease in strain to failure with increased aging time at 120°C. Insight to this behavior will come as the results of the bend-rupture tests are examined.

### 3.2.3 Bend-Rupture Data

Significant differences in bend-rupture behavior at elevated temperatures were discovered between two runs of the Baycomp carbon/PPS composite.

Bend-rupture tests at 90° C revealed large differences in time to rupture. Figure 3-2 shows these data with a log curve fit, Run 2 having order of magnitude shorter lives. The differences in bend-rupture behavior between the two runs are dramatic when compared to the small differences in quasi-static tensile behavior.

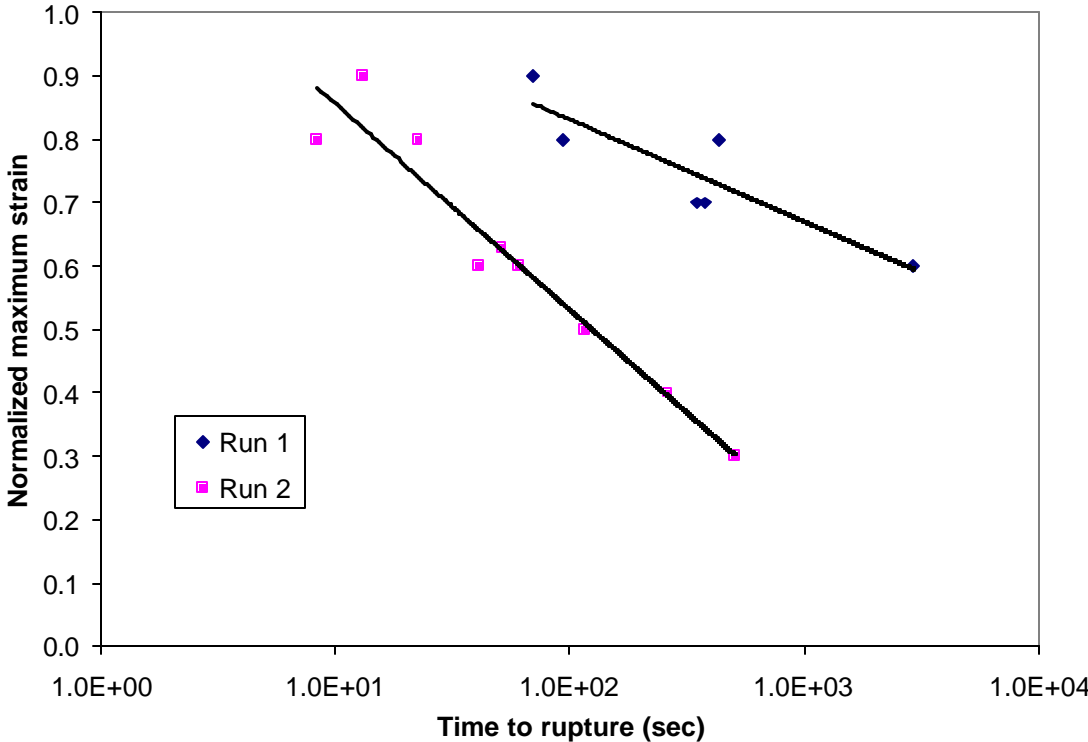


**Figure 3-2 90 °C Bend-rupture results for Run 1 and Run 2**

The bend-rupture loading condition requires the matrix to transfer load between broken fibers and the adjacent fibers on the tensile side of the specimen and also provide radial support to the fibers on the compression side. These results may indicate a difference in elevated temperature performance in other loading conditions, specially, where the matrix behavior plays an important role in the overall behavior of the material system.

### **3.2.4 Dynamic Mechanical Analysis**

A DMA investigation of the two runs was performed in an effort to explain the large differences in bend rupture behavior when compared to the quasi-static tension results. Two replicate DMA tests were performed on as received Run 1 and Run 2 materials. These tests show that the dominate relaxations of the material from the two runs differed by about 30° C. The first run had its dominate relaxation at 130° C and the second run at 103° C. Representative DMA results are shown in Figure 3-3 and Figure 3-4 respectively.

### 3.2.4.1 Run 1 DMA

There are several salient features in these results. The as received Run 1 DMA, Figure 3-3, exhibits a distinct shoulder on the  $\tan \delta$  curve at 100°C to the right of the dominant peak at 130°C. This represents the  $\beta$  and  $\alpha$  relaxations respectively. Examination of the  $\tan \delta$  curve shows a decrease in slope at 100°C indicating the  $T_g$  of the material. This result points to the possibility that there is more than one relaxation in the polymer matrix that may affect the behavior of the composite.

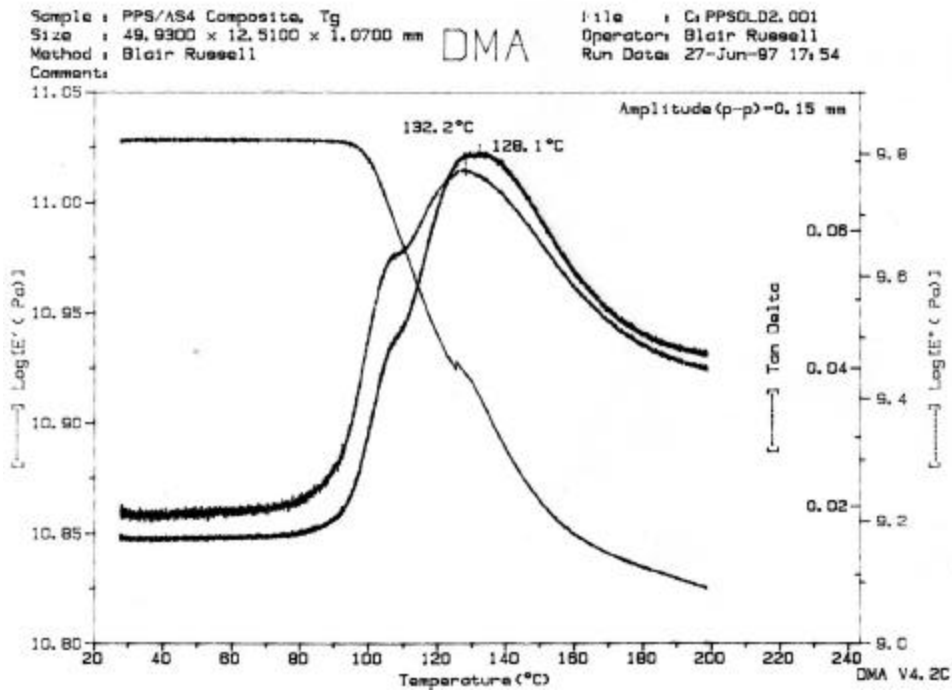


Figure 3-3 Representative DMA of Run 1 as received

### 3.2.4.2 Run 2 DMA

Figure 3-4 shows a narrow dominant peak at 103° C ( $\beta$  relaxation) with a secondary peak to its left at 130° C ( $\alpha$  relaxation). This result is perhaps more definitive as to the existence of multiple major relaxations in the PPS matrix. The secondary peak, at 130° C ( $\alpha$  relaxation), occurs at the temperature of maximum crystallinity,  $T_c$ , when the temperature is increased from below the  $T_g$ . This result is consistent with the previously cited literature. The primary peak of the as received Run 1 DMA also occurs at this temperature. Because the DMA test parameters are identical for both runs and the behavior during the test of each run is different, one must suspect that the initial crystallinity/morphology of the runs are different.

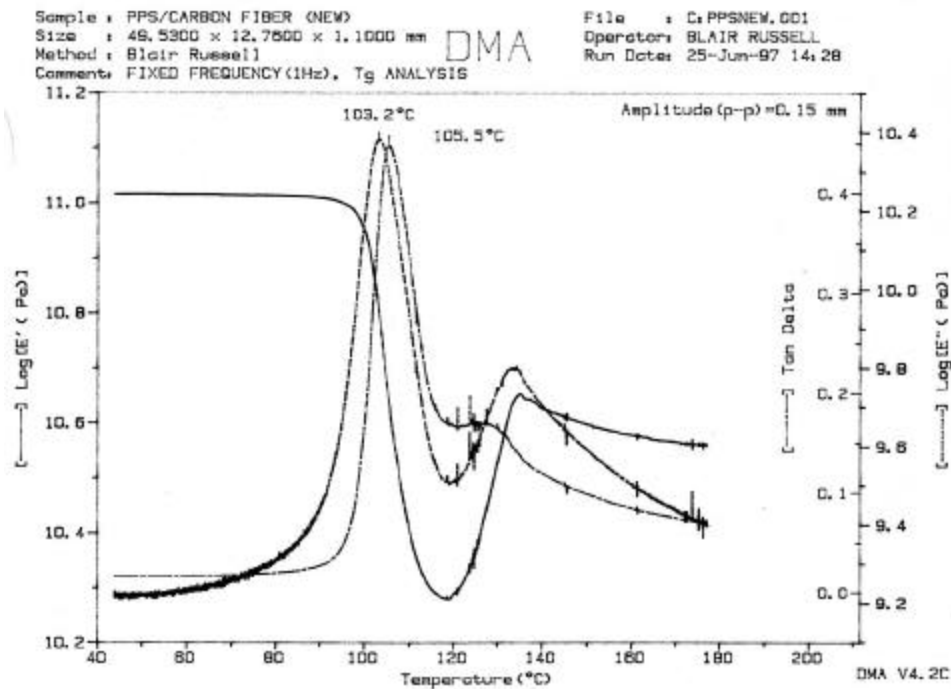
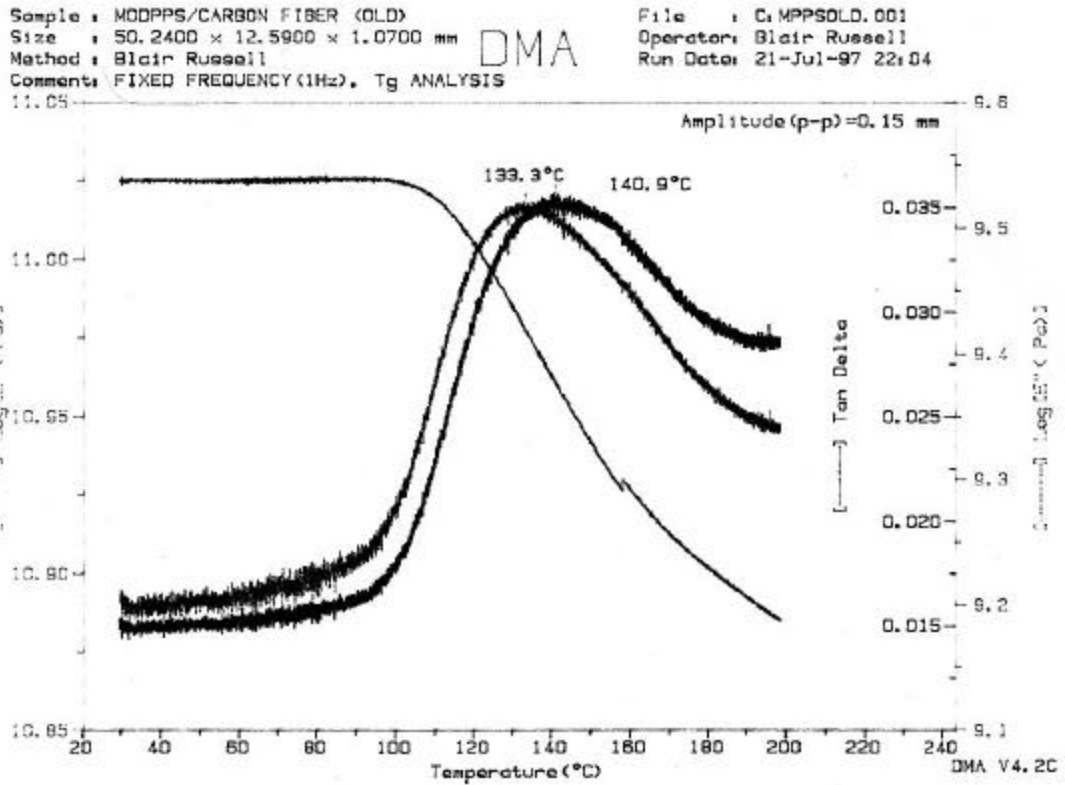


Figure 3-4 Representative DMA of batch 2 as received

Because PPS is a thermoplastic, differences in DMA results due only to differences in morphology of the matrix material should be reversible. These findings suggest that the performance of this material at elevated temperature is affected by PPS crystallinity/morphology.

### **3.2.5 Reprocessing Experiment**

An experiment was devised to determine if the differences in DMA results could be removed by reprocessing. DMA specimens from both Run 1 and Run 2 were prepared. The specimens were then placed in an oven and heated to 230° C. This temperature was chosen to be high in enough so that the PPS polymer chains could attain sufficient mobility to ‘erase’ most its original morphology and to not be so high that the composite would lose its consolidation. The material was held at 230° C for 60 minutes then quenched to 130° C in another oven for 60 minutes and then quenched to room temperature. A visual inspection of the specimens after reprocessing revealed no detectable change in color or shape between the two runs or between the pre and post-reprocessed material. Again, a DMA was performed on the specimens from the two runs. The results from these two tests, shown in Figure 3-5 and Figure 3-6, are almost identical, with their dominate relaxations at 130° C.



**Figure 3-5 DMA of batch 1 as modified**

The DMA results from the modified specimens are similar to the results from as received Run 1. From these results, it is believed that both runs of material are, indeed, made of identical constituents and the differences are caused primarily by differences in temperature profile during manufacturing.

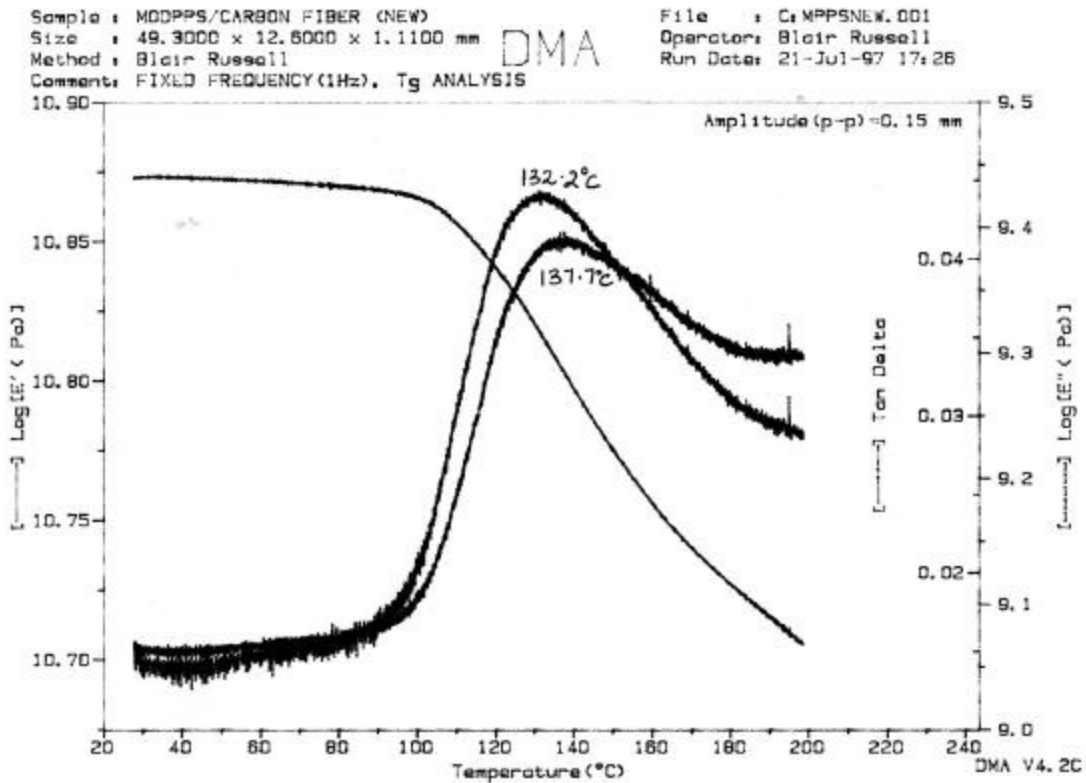


Figure 3-6 DMA of batch 2 as modified

### 3.3 Additional Runs

In a cooperative effort with the materials manufacturer, several additional runs were made with controlled processing parameters and examined using quasi-static tensile and bend-rupture tests. The three parameters that were varied in the additional runs were pull rate, cooling method and exit temperature. These parameters are defined in Table 3-6. All other adjustable parameters, such as die temperature, remained constant.

**Table 3-6 Processing parameter definitions**

<b>Parameter</b>	<b>Definition</b>	<b>Effect</b>
Pull rate	The rate measured between a point on the moving composite tape and a fixed point in the process, (m/min)	Controls residence time in cooling method and cooling rate within the specific additional cooling section of the process
Cooling method	Additional cooling method employed to reduce the temperature of the composite tape after consolidation	Effects the temperature differential and the heat transfer rate between the composite tape and the its surroundings
Ambient	Cooling method where composite tape was exposed only to the ambient conditions of the manufacturing plant (air @ ~23°C)	Slowest and most gradual cooling method, provides for the highest exit temperatures
Air	Cooling method where composite tape was exposed to chilled air via an inline refrigeration unit	Adds a rapid cooling period to the ambient cooling method, provides lower exit temperatures than ambient
Air/water	Cooling method where composite tape was exposed to chilled air via an inline refrigeration unit then additionally cooled in an inline chilled water bath	Adds a flash cooling period to the air cooling method, provides the lowest exit temperature and fastest cooling rate
Exit temperature	Temperature measured at the point after the additional cooling method was applied (Figure 3-1)	NA (measurement)

Nine additional samples were produced. Table 3-7 describes the processing parameters used in the manufacture of the additional samples.

**Table 3-7 Samples 1-9 processing parameters**

Sample	Pull Rate m/min	Cooling Method	Exit Temperature °C
Sample 1	20	Ambient	100
Sample 2	20	Air	70
Sample 3	20	Air/water	20
Sample 4	25	Ambient	120
Sample 5	25	Air	80
Sample 6	25	Air/Water	20
Sample 7	30	Ambient	125
Sample 8	30	Air	85
Sample 9	30	Air/water	25

Quasi-static tensile tests were performed on the Samples 4, 5, and 6 with a 25 m/min pull rate and also on Samples 1 and 7 which were also ambient cooled but run at a higher and lower pull rates. These results are given in Table 3-8.

**Table 3-8 Quasi-static test results**

		Modulus (msi)	Strength (ksi)	Strain to Failure (%)
Run 1	(10 replicates)	14.2	186	1.41
Run 2	(10 replicates)	14.7	196	1.39
Sample 1	(3 replicates)	15.5	209	1.41
Sample 2	(3 replicates)	-	-	-
Sample 3	(3 replicates)	-	-	-
Sample 4	(3 replicates)	14.0	189	1.40
Sample 5	(3 replicates)	14.3	209	1.52
Sample 6	(3 replicates)	14.5	200	1.41
Sample 7	(3 replicates)	14.9	195	1.43
Sample 8	(3 replicates)	-	-	-
Sample 9	(3 replicates)	-	-	-

Visual examination of Samples 1-9 indicated non-uniform wet-out of fibers across the width of the tape. Although hard to quantify, the severity of this problem seemed to be consistent through all nine samples. It is unclear to the author whether this problem was related to the processing parameters or to the extremely short trial runs used to produce these samples. These matrix-poor regions caused longitudinal splitting in several of the bend-rupture test specimens during testing.

Figure 3-7 shows the bend-rupture test results for Samples 4, 5, and 6 along with the data from Run 1 and Run 2 for comparison. Because of the time constraint, these tests were run at high strain levels so that a reasonable number of data points could be collected.

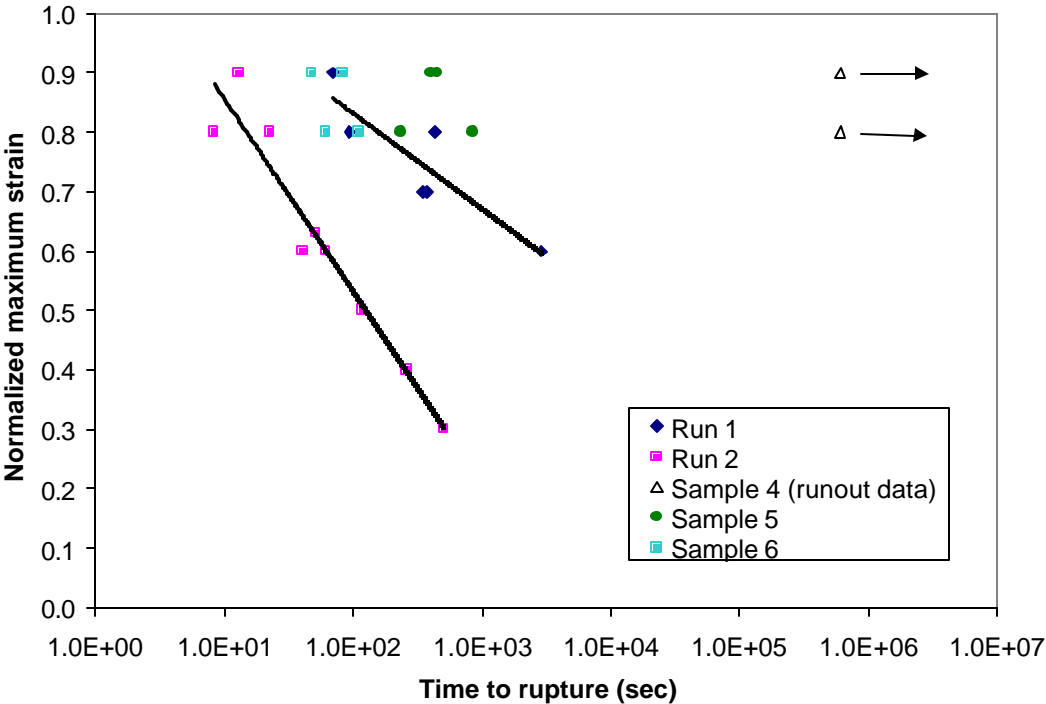


Figure 3-7 90 °C Bend-rupture results for Samples 4, 5, 6 and Run 1 and Run 2

The most interesting result from these tests is the bend rupture life of Sample 4. Two data points are shown in Figure 3-7 for Sample 4. These points indicate the duration of a test that was stopped before the specimen failed (runout). In the case of Sample 4 specimens had not experienced failure after a duration 3 orders of magnitude beyond the last failure of Run 1, Run 2, Sample 5 and Sample 6. A review of the processing parameters reveals that Sample 4 had the highest exit temperature, 120°C, of these samples and the slowest cooling rate, ambient cooling. These results are consistent with the previously cited literature.

### **3.4 Summary: Chapter 3**

A pultruded carbon fiber/PPS semicrystalline thermoplastic matrix composite has been discussed. Contrasting quasi-static tensile and bend-rupture results were presented for two runs of the composite with identical constituents. Bend-rupture results differed by orders of magnitude between the two runs. Run 1 material gained strength after aging at elevated temperatures. Through DMA testing, differences in the relaxation profiles of the matrix materials were revealed. The two runs of material were then reprocessed and DMA tests produced identical results for the reprocessed Run 1 and Run 2 material. Differences in the crystallinity/morphology of the PPS were indicated as the primary cause of the discrepancies in mechanical behavior between the two runs. A study of the effects of varying processing parameters on the tensile and bend-rupture behavior of the composite was conducted. A correlation has been shown between the pultrusion processing parameters and the mechanical properties of this carbon fiber/PPS composite. These results underline the importance of process control to insure that a consistent product is produced. This study also presents the possibility that mechanical properties may be optimized through the control of processing parameters to improve elevated temperature behavior.

## Chapter 4

### 4 TENSILE STRENGTH AND TENSILE RUPTURE BEHAVIOR

The tensile properties of the carbon fiber/PPS composite are of particular importance to its use in non-bonded flexible risers. Traditional tensile armor service is dominated by tension and in the present case, because of the slenderness of the composite wire; additional care is taken in the riser design to eliminate as much compression as possible. In the present chapter, a few additional comments are made concerning the tensile behavior of the composite, the initial statistical tensile strength distributions are presented for several cases and are compared to the strength models discussed in Chapter 1. Preliminary tensile rupture data are also presented and discussed.

#### 4.1 Initial Tensile Strength

In the case of predicting static strength of a material consisting of parallel continuous fibers contained in a matrix material, commonly referred to as a unidirectional composite, several models have been suggested. As a first approximation, the fiber direction strength of a unidirectional composite can be estimated by assuming that the two constituents, fiber and matrix, contribute to the strength of the composite in relation to their fiber volume fraction,  $V_f$  [31]. The Rule of Mixtures (ROM) strength is given by

$$X_t = X_f V_f + X_m (1 - V_f) \quad (30)$$

where  $X_t$  is the composite tensile strength,  $X_f$  and  $X_m$  are the tensile strengths of the fiber and matrix respectively.

Table 4-1 presents statistical fiber strength data for AS4 carbon fibers. Further analysis of this data yields;  $m = 10.65$ ,  $\sigma_0 = 760.9$  ksi,  $L_0 = 0.394$  in. Although the fibers in the present composite are not Hercules AS4 but Grafil 34-700 fibers, both fibers are intermediate modulus fibers and the author was unable to find statistical data for the present fibers. This data is used in the following strength models.

**Table 4-1 Weibull reference strength for various gage lengths[32]**

Gage Length (in)	Weibull Reference Strength $S_0$ (ksi)
1.97	552
1.18	558
0.79	574
0.24	645
0.12	683

As a further attempt, the composite can be thought of as a bundle of fibers with no contribution to the strength from the matrix. As reviewed in Chapter 1 the strength of a bundle of fibers of length L is given by

$$X_t = V_f E_f e_0 \left( \frac{L_0}{mLe} \right)^{\frac{1}{m}} \tag{31}$$

where  $E_f$  is the stiffness of the fibers,  $e_0$ ,  $L_0$ , and  $m$  are Weibull parameters. This estimate may be modified to include some influence of the fiber matrix interaction (although unnatural) by replacing the bundle length, L, by an ineffective length,  $\delta$ . In this case,  $\delta$  is the length over which a broken fiber carries no load and therefore influences its neighboring fibers.

One of the most widely used models for tensile strength of unidirectional composite materials is Batdorf's [33,34] model. In his model, he considers the only damage in the composite to be fiber failure. The matrix only contributes as a means to introduce a stress concentration

on adjacent fibers over an ineffective length. As load increases on the composite, the weakest fiber fails and sheds its stress to its neighbors increasing the probability that a neighboring fiber, in the plane of the initial break, will fail. The single fiber break (singlet) becomes a double fiber break (doublet) and so on. As the load is increased this process continues to the point of instability and ultimate failure of the composite. The lowest stress at which an arbitrary number of broken fibers becomes unstable defines the strength of the composite.

Of late Monte Carlo simulations for the strength of unidirectional composites [35] have been gaining acceptance. These simulations are a technique for obtaining the strength distributions of unidirectional composite systems. Table 4-2 shows the strength results obtained from rule of mixtures, bundle strength calculations, Batdorf’s analysis, and the Monte Carlo simulations. Like Batdorf’s analysis, the Monte Carlo simulations require the Weibull statistics for the strength of the fibers, the modulus of the fiber and matrix, the fiber volume fraction, fiber diameter and packing arrangement.

**Table 4-2 Strength models compared to experimental results.**

	<b>Strength, ksi</b>	<b>Weibull shape parameter</b>
Rule of mixtures	267	–
Bundle Strength	148	–
Batdorf	232	–
Monte Carlo simulation	265	82.0
<b>[36]</b>		
Experimental	227	19.8

The Batdorf technique and the Monte Carlo simulations over-estimate composite strength. Although the Batdorf results are closer to the experimental strength, the Monte Carlo strength simulations more accurately mimic the progression of fiber breaks leading up to

composite failure. In the Batdorf analysis, the breaks are assumed to be co-planar. Since this limitation is not imposed in the Monte Carlo simulations, the Batdorf strength is lower than the Monte Carlo simulation result for strength. Moreover, the Batdorf analysis imposes a linear approximation to the stress profile in the overstressed region on fibers surrounding a break cluster. This technique overestimates the stresses on unbroken fibers, which in turn lowers the strength prediction from a Batdorf analysis. Also, the Monte Carlo simulation yields Weibull statistics for failure of the composite from the Weibull fiber strength distribution.

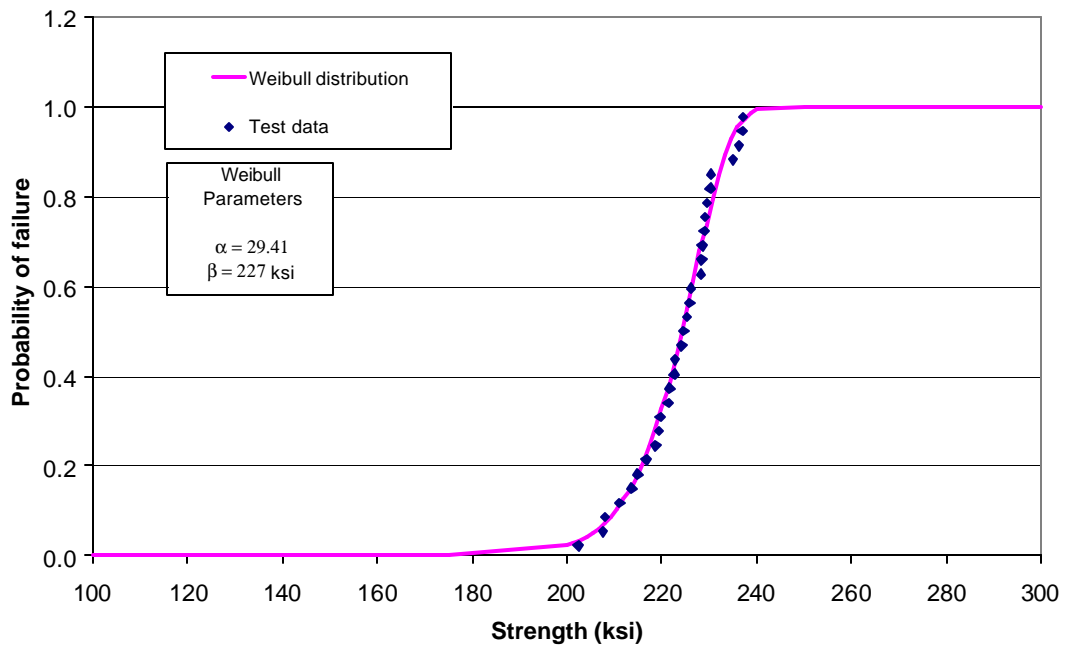
## **4.2 Weibull Tensile Strength Distribution**

The quasi-static tensile strength data sets were obtained experimentally. Approximately 30 tests were run for each of three cases. These cases consisted of the following material:

- Material from 1 run of the carbon fiber/PPS composite as received
- Material from 6 runs of the carbon fiber/PPS composite as received
- Material from 6 runs of the carbon fiber/PPS composite aged 21 days in 90° C saltwater

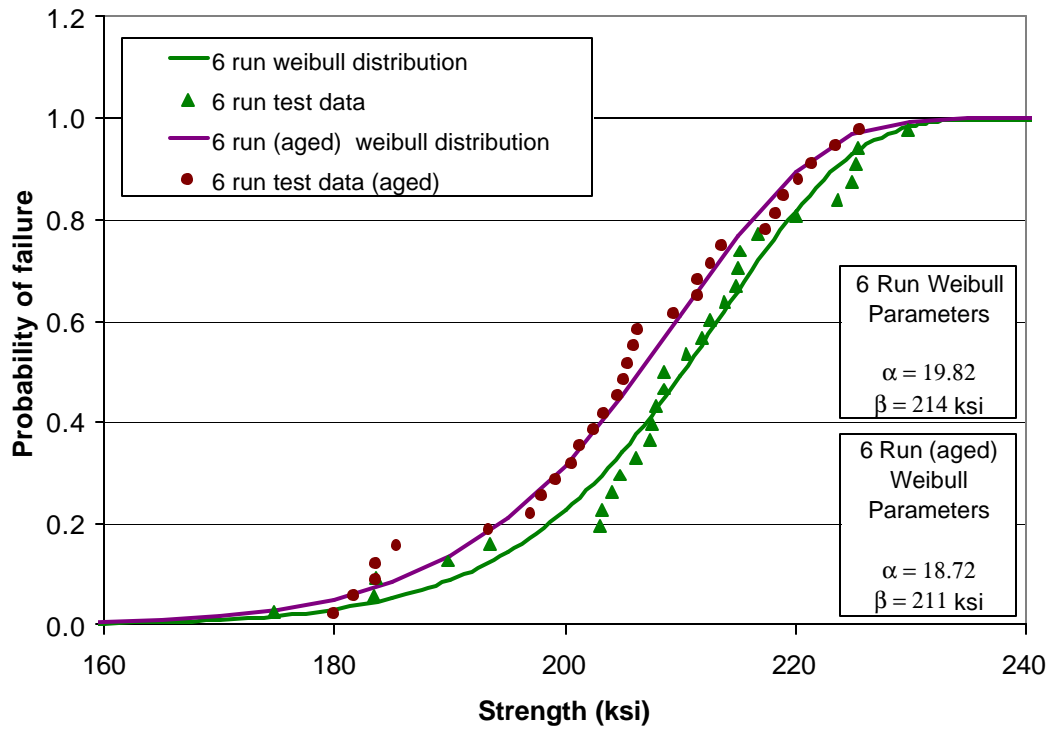
Figure 4-1 shows the probability of failure of a single manufacturing run of the composite with increasing load.

Figure 4-1 illustrates the consistent strength of the composite with in a single run which maybe expected due to manufacturing method. This data also supports the reproducibility of the quasi-static tensile test method.



**Figure 4-1 Probability of failure for material from 1 run of the carbon fiber/PPS composite as received**

Quasi-static tensile strength results are presented in Figure 4-2 for six runs of material before and after aging. Each data set consisted of 5 specimens from each run. It may be argued that these 6 runs can be identified within the distributions. Further statistical analysis is necessary to confirm this.



**Figure 4-2 Probability of failure for material from 6 runs of the carbon fiber/PPS composite as received and aged**

Figure 4-3 shows the widening of the distributions between the 1 run data set and the 6 run data set, and the larger deviation from the Weibull distribution.

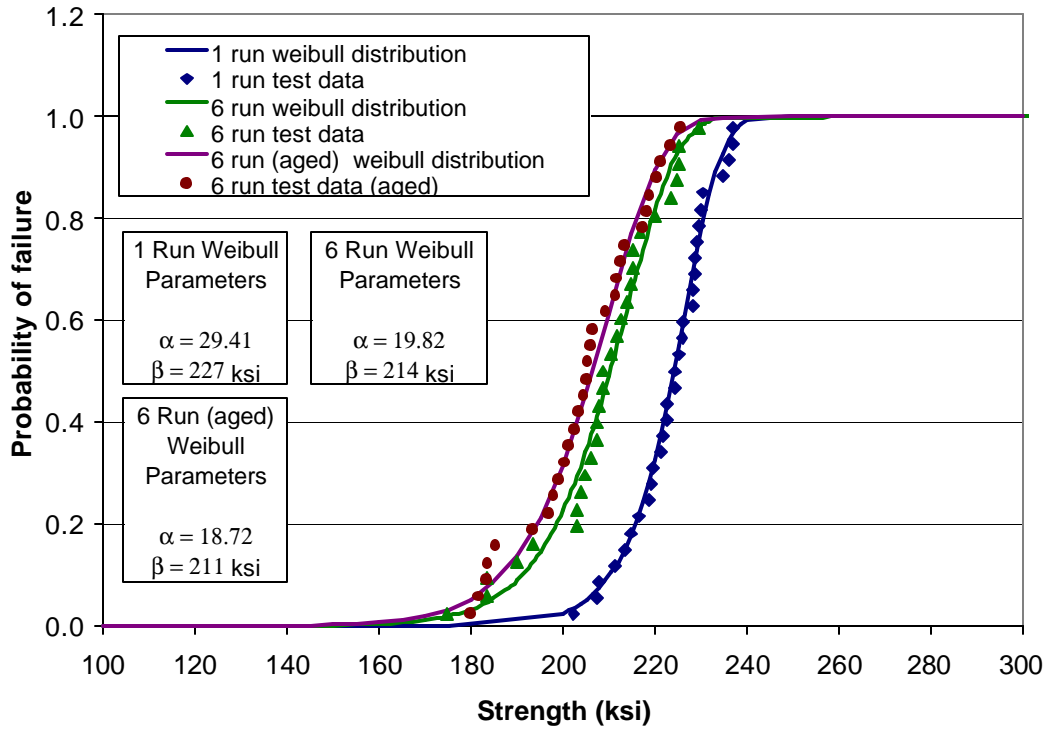


Figure 4-3 Comparison of probability of failure for three cases

### 4.3 Tensile Rupture Behavior

Understanding the tensile rupture behavior of the composite is important to its use in non-bonded flexible risers. The relationship between the time to rupture and the applied stress and temperature are necessary inputs to the life prediction methodology presented in Chapter 5. Because of the difficulty in conducting tensile rupture tests, limited data is available. The limited data collected in the current study was fit by the form

$$t_{rupture} = e^{A+B/T+Ds} \quad (32)$$

where A, B, and D are fitting parameters and  $t_{rupture}$  and  $\sigma$  are the time to rupture and applied normalized stress respectively. Figure 4-4 shows the rupture curve fits for 90, 80, and 70 °C at normalized stresses of 90.0% and 87.5% of the Weibull strength of the Case 1 composite. The high load levels and temperatures tested were dictated by the limited amount of time available to conduct tests.

It is evident from Figure 4-4 that longer tests at lower temperatures and stress levels are

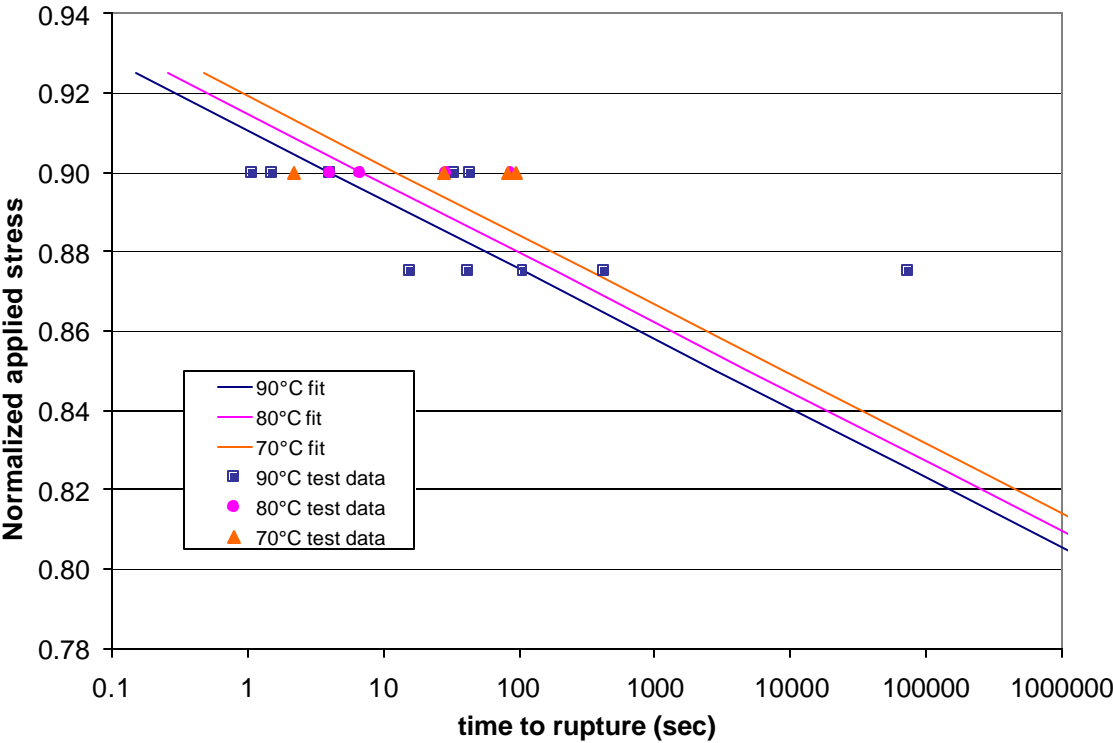


**Figure 4-4 Time to rupture at temperature**

required to measure the load and temperature dependence of the tensile rupture behavior. This fact further motivates the use of a test method like the bend rupture method to determine time dependent behavior.

## **Summary: Chapter 4**

Chapter 4 several features concerning the tensile behavior of the carbon fiber/PPS composite. Tensile strength models were compared to experimental results of one run of composite. The Weibull strength distributions for three cases were presented and compared and demonstrated expected results. The difficulty in obtained tensile rupture results was discussed.

## Chapter 5

### 5 FATIGUE – RUPTURE COMBINED LOADING

Combinations of failure mechanisms are frequently encountered in the life prediction of composite materials. In the present chapter, a life prediction methodology is developed and applied to one such failure mechanism combination. This method uses experimental data and analytical tools to predict the long-term behavior of a composite under service conditions. The prediction scheme is based on the assumption that damage accumulation progressively reduces the remaining strength of a composite. An overview of the fundamental concepts of the life prediction method is presented. The method is used to model the elevated temperature fatigue behavior of the unidirectional Grafil 34-700 carbon fiber/ polyphenylene sulfide (PPS) matrix composite previously discussed. The nonlinear combined effects of time at elevated temperature and fatigue are taken into account by considering elevated temperature tensile rupture and room temperature fatigue behavior. The life prediction for the combined loading is compared to 90°C tensile-tensile fatigue data. This comparison shows good correlation between the predictions and data, and thereby demonstrates the method's effectiveness in life prediction modeling.

Life prediction of composite materials subjected to combined loading is often a key aspect of design. Combined loads may be comprised of quasi-static mechanical loads (tension, compression, shear, etc.), mechanical fatigue, elevated temperatures, thermal cycling and chemical degradation. It is usually not possible to include all of these factors and their variations in a single test. Therefore it is necessary to have an analytical method for combining the applicable conditions to predict the life of composites.

In order to use this material for the flexible riser application described in Chapter 1, the service life prediction must include the effects of fatigue and elevated temperatures up to 90°C. The service life model for the material under consideration was constructed using the methodology proposed by Reifsnider et al [37]. This methodology has been used for a variety of material systems in many service environments and has been integrated into a performance simulation code, MRLife, developed by the Materials Response Group at Virginia Tech [38, 39, 40]. This methodology uses experimental data and analytical tools to predict the long-term behavior of a composite. The method is verified for the current material via comparison of experimental data to the predicted life.

## **5.1 Life Prediction Overview**

The present life prediction scheme is based on damage accumulation concepts applied to composite materials. The basic principles of this scheme are described as follows. We begin our analysis by postulating that remaining strength may be used as a damage metric [37-41]. We next assume that the remaining strength may be determined (or predicted) as a function of load level and some form of generalized time. For a given load level, a particular fraction of life corresponds to a certain reduction in remaining strength. We claim that a particular fraction of life at a second load level is equivalent to the first if (and only if) it gives the same reduction in remaining strength, as illustrated in Figure 5-1. In the case of Figure 5-1, time  $t_1$  at an applied stress level  $S_a^1$  is equivalent to time  $t_2$  at stress level  $S_a^2$  because it gives the same remaining strength. In addition, the remaining life at the second load level is given by the amount of generalized time required to reduce the remaining strength to the applied load level. In this way, the effect of several increments of loading may be accounted for by adding their respective reductions in remaining strength. For the general case, the strength reduction curves may be nonlinear, so the remaining strength and life calculations are path dependent.

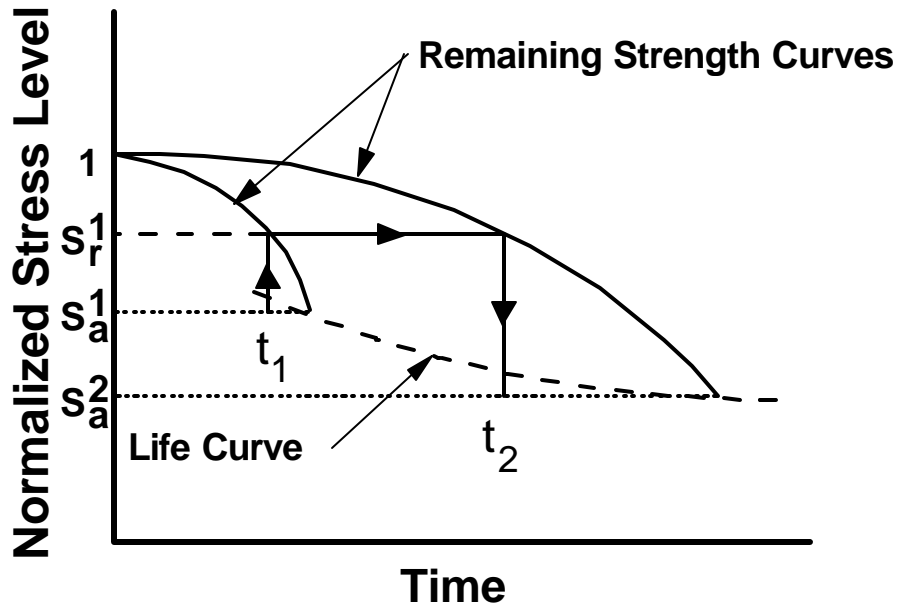


Figure 5-1 The use of remaining strength as a damage metric

Our next step in the analysis is to postulate that normalized remaining strength (our damage metric) is an internal state variable for a damaged material system. This normalized remaining strength is based on the selection of an appropriate failure criterion (such as maximum stress or Tsai-Hill) which is a scalar combination of the principal material strengths and applied stresses in the critical element. In this way we are able to consider a single quantity rather than the individual components of the strength tensor. In the present case, a maximum stress criterion is chosen as the failure function for the unidirectional composite loaded in axial tension. We denote this failure function by  $Fa$ . We next construct a second state variable, the continuity [42], defined as  $(1-Fa)$  and denote it by  $y$ . We shall attempt to define our remaining strength and life in terms of  $y$ . To do so, we assume that the kinetics are defined

by a specific damage accumulation process for a particular failure mode, and assign appropriate rate equations to each of the processes that may be present.

For the present case, we assume that a common kinetic equation (a power law) describes the damage accumulation in our material such that

$$\frac{dy}{dt} = -Ayj\mathbf{t}^{j-1} \quad (1)$$

where

$\psi$  = continuity

$\tau$  = generalized time variable

A = constant

j = material parameter

The generalized time,  $\tau$ , is defined by

$$\mathbf{t} = \frac{t}{\hat{t}} \quad (2)$$

where

t = time

$\hat{t}$  = characteristic time

The characteristic time could be a creep rupture life, a creep time constant, or a fatigue life, in which case

$$\mathbf{t} = \frac{n}{N} \quad (3)$$

where

$n$  = number of fatigue cycles

$N$  = number of cycles to failure for the applied loading condition

Next, we rearrange Equation (1) and integrate so that we have

$$\int_{y_o}^{y_i} dy = -A \int y j t^{j-1} dt \quad (5)$$

If we integrate the left-hand side and substitute  $(1-Fa)$  for  $y$  we have

$$y_2 - y_1 = Fa_1 - Fa_2 = -\Delta Fa \quad (6)$$

Next, we define our normalized remaining strength,  $Fr$  so that

$$Fr = 1 - \Delta Fa = 1 - A \int_0^t (1 - Fa) j t^{j-1} dt \quad (7)$$

For loading cases in which  $Fa$  is constant, Equation (7) may be integrated to obtain

$$Fr = 1 - A(1 - Fa)t^j \quad (8)$$

The point at which  $Fr$  is equal to  $Fa$  defines material failure. Based upon the definition of  $t$ , for the constant amplitude case this condition should occur when  $\tau$  is equal to unity, so that  $A$  is also equal to unity. The resulting evolution equation for the remaining strength is then given by

$$Fr = 1 - \Delta Fa = 1 - \int_0^t (1 - Fa) j t^{j-1} dt \quad (9)$$

The material parameter,  $j$ , is related to the shape of the remaining strength curve [3]. The parameter,  $j$ , can be determined from remaining strength data for a given failure mechanism. In our case  $j$  was chosen to be 1.2 based on previous experience with carbon/polymer composites.

Equation (9), which is a direct result of the kinetic equation given in Equation (5) has been used with a great deal of success for polymer composites [21-24] under fatigue loading conditions. Recently, an approach has been developed to predict the lifetime under combined fatigue and rupture conditions [43]. This approach is used in the present work.

## 5.2 Method Validation

We will now apply the damage accumulation scheme previously described to predict the elevated temperature fatigue behavior of the material under study and then compare these predictions to experimental data.

### 5.2.1 Tensile Rupture

The first step in implementing the method for this task is to characterize the time dependent behavior of the failure process. In our case, this is tensile rupture at an elevated temperature of 90°C.

An equation presented by Kachanov [42] of the form

$$t_{rupture} = \frac{1}{(n+1) \cdot B \cdot Fa^n} \quad (10)$$

where

$Fa = \mathbf{s}/\mathbf{s}_{ult}$  = applied stress/ultimate strength

$t_{rupture}$  = time to rupture in hours

B, n = constants determined through curve fitting

is used to describe the tensile rupture behavior. Setting  $\sigma$  equal to  $S_r$  (the remaining strength fraction) Equation (10) can be rewritten in the form

$$Fa = \left[ \frac{1}{(n+1) \cdot B \cdot t_{rupture}} \right]^{\frac{1}{n}} \quad (11)$$

Equation (10) was fit, using a least squares method, to 90°C tensile rupture data for the present material. The values of  $B$  and  $n$  were determined to be 0.0382 and 26.0, respectively (for the time to failure given in seconds). The tensile rupture curve fit and data are shown in Figure 5-2.

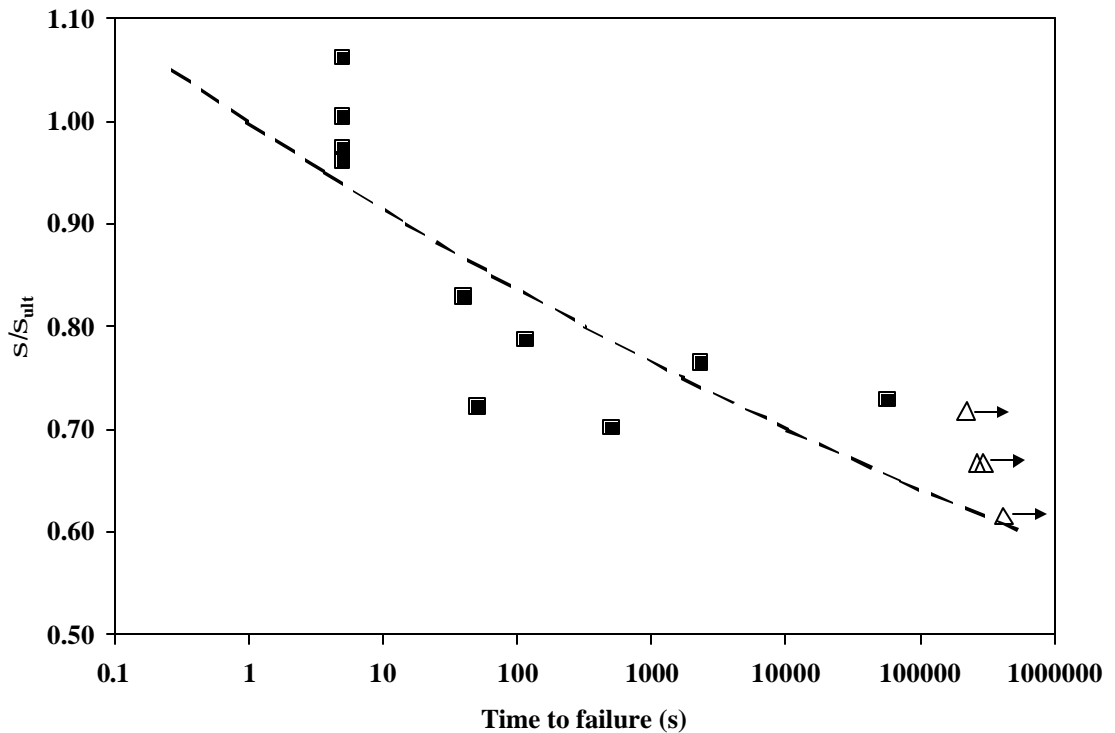


**Figure 5-2 Tensile rupture curve fit and data**

### 5.2.2 Fatigue

Next, the fatigue effect of the combined loading was characterized. The room temperature fatigue data were fit with a conventional S-N curve of the form

$$\frac{S}{S_{ULT}} = A_n + B_n (\log N)^{P_n} \quad (12)$$

where

$S/S_{ult}$  = normalized maximum stress

$N$  = number of cycles to failure

$A_n, B_n, P_n$  = material constants

The data and curve are shown in Figure 5-3. The constants were found to be:  $A_n=0.9207$ ,  $B_n=-0.0189$ , and  $P_n=1$ .

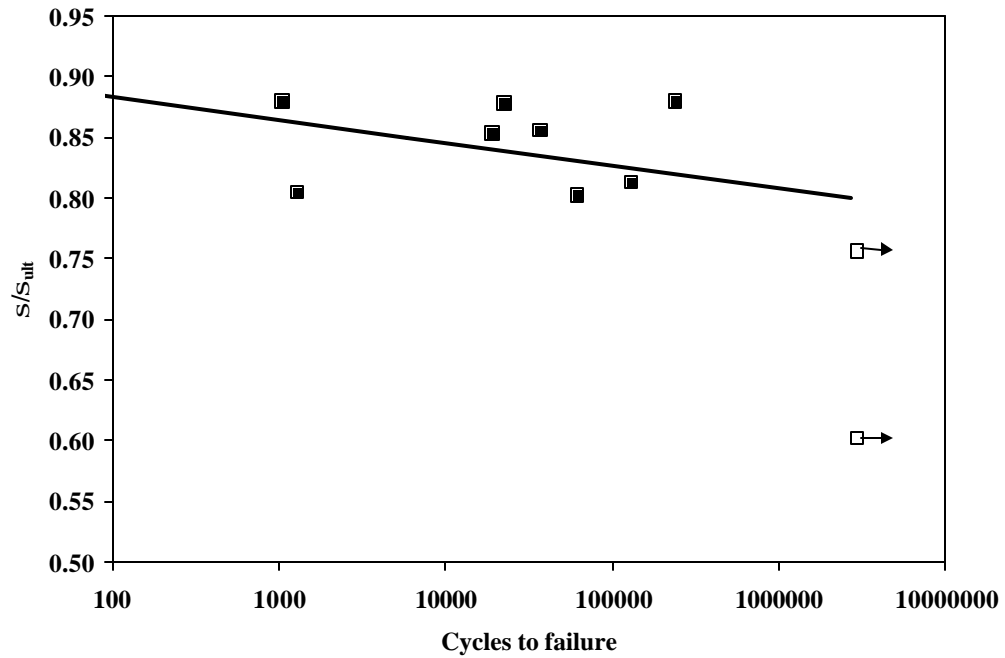


**Figure 5-3 Room temperature fatigue data and S-N curve fit**

### 5.2.3 Combined Rupture and Fatigue

Finally, the effects of time at elevated temperature and fatigue were combined by defining a characteristic time as described previously in reference [6]. The prediction for the combined loading and the 90°C fatigue data show a good agreement (Figure 5-4). This verifies the technique for predicting the combined effects of time and cyclic processes for the material and conditions under study.

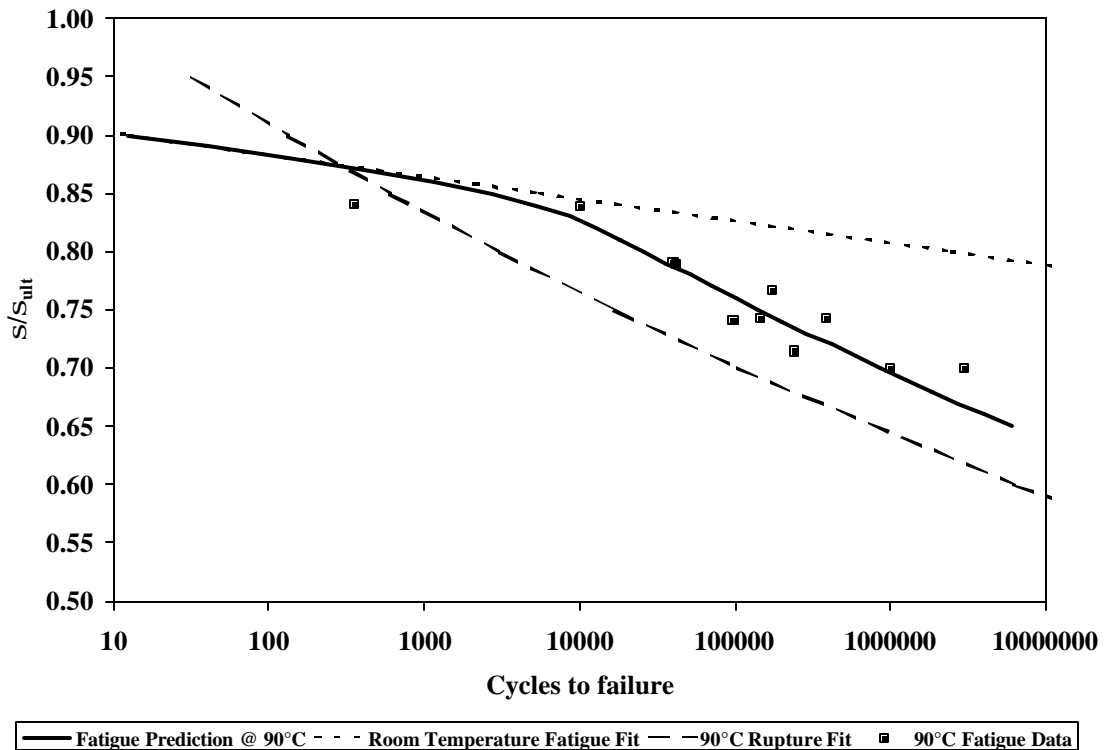


Figure 5-4 Comparison of elevated temperature fatigue prediction and 90°C fatigue data

### 5.3 R-Ratio Influence

For the present case, tension-tension ( $R = 0.1$ ) fatigue of a unidirectional composite at elevated temperature, this method resulted in a good prediction of life under present combined loading. It is expected that for tension-tension fatigue loading with other R-ratios, the present characterization of the fatigue effect on life will produce similarly good predictions. This should be confirmed through experiment. As the failure mechanism is expected to be different for tension-compression or compression-compression fatigue this failure mechanism would need to be characterized in order represent the fatigue effect in this method.

## **5.4 Summary: Chapter 5**

The life prediction model presented is based on an iterative strength reduction scheme, which allows for the consideration of several types of combined generalized loads and applied environments. This paper studied only environmental conditions and cyclic loading; however, any number of other load types may be able to be combined using a similar technique. Comparison of experimental data with the life prediction results has demonstrated the model's effectiveness for the material and loading case under study.

## Chapter 6

### 6 CONCLUSIONS

Several key findings produced during the research and development of a carbon fiber/thermoplastic matrix composite intended to replace a steel component in a non-bonded flexible riser have been presented. These findings include the introduction of a bend-rupture test method that proves to be simple to implement and sensitive to subtle differences in the matrix material of composites. In addition, the importance of manufacturing processing parameters on the long-term behavior of a semicrystalline thermoplastic matrix composite has been illuminated. Experimentally determined static strength, and tensile rupture data are presented as a basis for future life prediction modeling. A remaining strength approach for life prediction has been developed and presented for the case of combined fatigue and rupture loading.

The context in which the present work was undertaken along with the foundation that this work extends has been made clear. The motivation to use composite materials in a non-bonded flexible riser for use in the offshore oil industry was put forth. The requirements for such a material were detailed.

A pultruded carbon fiber/PPS semicrystalline thermoplastic matrix composite has been discussed. Contrasting quasi-static tensile and bend-rupture results were presented for two runs of the composite with identical constituents. Bend-rupture tests produced results that differed by orders of magnitude between the two runs. The bend-rupture test method results proved to be the most sensitive to the differences in the thermoplastic matrix composite. Run

1 material gained strength after aging at elevated temperatures. Through DMA testing, differences in the relaxation profiles of the matrix materials were revealed. The two runs of material were then reprocessed and DMA tests produced identical results for the reprocessed Run 1 and Run 2 materials. Differences in the crystallinity/morphology of the PPS were indicated as the primary cause of the discrepancies in mechanical behavior between the two runs. A study of the effects of varying processing parameters on the tensile and bend-rupture behavior of the composite was conducted. A correlation has been shown between the pultrusion processing parameters and the mechanical properties of this Carbon fiber/PPS composite. These results underline the importance of process control to insure that a consistent product is produced. This study also presents the possibility that mechanical properties may be optimized through the control of processing parameters to improve elevated temperature behavior.

The life prediction model presented is based on an iterative strength reduction scheme, which allows for the consideration of several types of combined generalized loads and applied environments. The present work studied only environmental conditions and cyclic loading; however, any number of other load types may be able to be combined using a similar technique. Comparison of experimental data with the life prediction results has demonstrated the model's effectiveness for the material and loading case under study.

## REFERENCES

- [1] M. D. Kalman, J.R. Belcher, “Flexible Risers with Composite armor for Deepwater Oil and Gas Production,” *Progress in Durability Analysis of Composite Materials*, 1998 Balkema press pp 41-48
- [2] M. D. Kalman, T. Blair, M. Hill, P. Lewicki, C. Mungall, and B. Russell, “Composite-Armored Flexible Riser System for Oil-Export Service,” *Offshore Technical Conference*, May 1999
- [3] K. L. Reifsnider, S. W. Case, “Mechanics of Composite Strength and Life, ESM 6104” Class notes Virginia Tech
- [4] Batdorf, S. B. “Tensile Strength of Unidirectionally Reinforced Composites—I,” *J. Reinforced Plastics and Composites*, **1** (1982), 153-164.
- [5] Batdorf, S. B. “Tensile Strength of Unidirectionally Reinforced Composites—II,” *J. Reinforced Plastics and Composites*, **1** (1982), 165-176.
- [6] Landis, M. L., Beyerlein, I. J., McMeeking, R. M. “Micromechanical simulation of the failure of fiber reinforced composites,” *Journal of the Mechanics and Physics of Solids*, Vol. 48, 2000, p. 621-648.
- [7] Gao, Z. and Reifsnider, K.L., “Micromechanics of Tensile Strength in Composite Systems,” *Composite Materials; Fatigue and Fracture, Fourth Volume, ASTM STP 1156*, (1993), pp. 453-470.
- [8] Boyd, R, H, “Relaxation Processes in Crystalline Polymers: experimental behavior – a review,” *Polymer* , 1985, Vol 26, March pp. 323-347
- [9] Boyd, R, H, “Relaxation Processes in Crystalline Polymers: molecular interpretation – a review,” *Polymer* , 1985, Vol 26, August pp. 1123-1133
- [10] Mahieux, C, L, Reifsnider, K, L, “Influence of temperature on the durability of polymer matrix composites,” American Society of Mechanical Engineers, 1999 ASME Mechanics & Materials Conference Final Program & Book of Abstracts (USA), pp. 127-128, June 1999

- [11] Talbott, Springer, Berglund, “The Effects of Crystallinity on the Mechanical Properties of PEEK Polymer and Graphite Fiber Reinforced PEEK,” *Journal of Composite Materials* Vol 21, Nov 1987
- [12] I. M Ward, D.W. Hadley, “An introduction to the Mechanical Properties of Solid Polymers,” John Wiley & Sons, New York 1993 pp 62-64
- [13] B. E. Russell, C. Mahieux, and K. L. Reifsnider, “Stress Rupture of PMC’s in End-Loaded Bending,” *Journal of Applied Composites*. 1998, Vol. 5, No. 3, 151-159.
- [14] ASM International Handbook Committee, *Metals Handbook*, 1985, v 8 pp 503
- [15] Fukuda H 1989 “A New Bending Test Method of Advanced Composites” *Exp. Mech.*, 29 (4): pp 330-335
- [16] Fukuda H., Katoh H., Uesugi, H., “A Modified Procedure to Measure Bending Strength and Modulus of Advanced Composites by Means of Compression Bending. *Journal of Composite Materials*, vol. 29, no. 2/1995, pp 195-207
- [17] Timoshenko, S. P. and Gere, J. M. 1961 *Theory of Elastic Stability*, Second Ed. McGraw-Hill, pp.76-82
- [18] C. Mahieux, B. E. Russell, and K. L. Reifsnider, “Stress Rupture of Unidirectional Polymer Matrix Composites in End-Loaded Bending at Elevated Temperatures, Part I: Experimental Characterization of the Failure Mode,” *Journal of Composite Materials*, 1998, Vol. 32, No. 14, 1311-1321.
- [19] C. Mahieux, B. E. Russell, and K. L. Reifsnider, “Stress Rupture of Unidirectional Polymer Matrix Composites in end loaded bending at Elevated Temperatures, Part II: Analytical,” *Journal of Composite Materials*, 1999, Vol. 33, No. 1, 22-37.
- [20] Loverich, J, “Life Prediction of Composite Armor in an Unbonded Flexible Pipe” Master’s Thesis, Virginia Tech, 1997
- [21] Reifsnider, K. L. and W.W. Stinchomb, “A Critical Element Model of the Residual Strength and Life of Fatigue Loaded Coupons,” *Composite Materials: Fatigue and Fracture*, ASTM STP 907, Edited by H. T. Hahn, ASTM, (1986), 298-303.
- [22] Case, S.W. and Reifsnider, K.L., *MRLife11<sup>TM</sup> A strength and Life Prediction Code for Laminated Composite Materials*, Materials Response Group, Virginia Tech, (1998).

- [23] Reifsnider, K.L., "Use of Mechanistic Life Prediction Methods for the Design of Damage-Tolerant Composite Material Systems," *Advances in Fatigue Lifetime Predictive Techniques: Second Volume, ASTM STP 1211*, (1993), pp. 3-18.
- [24] Reifsnider, K., Case, S., and Iyengar, N., "Recent Advances in Composite Damage Mechanics," *Proceedings of Conference on Spacecraft Structures, Materials & Mechanical Testing* (ESA SP-386), Noordwijk, The Netherlands, June 1996, pp. 483-490.
- [25] J. S. Loverich, B. E. Russell, S. W. Case, and K. L. Reifsnider, "Life Prediction of PPS Composites Subjected to Cyclic Loading at Elevated Temperatures," Time Dependent and Nonlinear Effects in Polymers and Composites, ASTM STP 1357, 1999.
- [26] ASTM D 3039
- [27] ASTM D 3479
- [28] B. E. Russell, C. Mahieux, and K. L. Reifsnider, "Stress Rupture of PMC's in End-Loaded Bending," *Journal of Applied Composites*. 1998, Vol. 5, No. 3, 151-159.
- [29] Grafil 34-700 Standard Modulus Carbon fiber data sheet
- [30] Phillips Petroleum Company Ryton Data Sheet
- [31] Kelly, A. and Nicholson, R.B. (eds.) *Strengthening Methods in Crystals*, Elsevier Pub. London, (1971).
- [32] Wimolkiasak, A. S.; Bell, J. P., "Interfacial Shear Strength and Failure Modes of Interphase-Modified Graphite--Epoxy Composites" *Polymer Composites* 10(3), 1989, 162-172
- [33] Batdorf, S. B. "Tensile Strength of Unidirectionally Reinforced Composites—I," *J. Reinforced Plastics and Composites*, **1** (1982), 153-164.
- [34] Batdorf, S. B. "Tensile Strength of Unidirectionally Reinforced Composites—II," *J. Reinforced Plastics and Composites*, **1** (1982), 165-176.
- [35] Landis, M. L., Beyerlein, I. J., McMeeking, R. M. "Micromechanical simulation of the failure of fiber reinforced composites," *Journal of the Mechanics and Physics of Solids*, Vol. 48, 2000, p. 621-648.

- [36] Tozer Bandorawalla, *personal communication October 2000*
- [37] Reifsnider, K. L. and W.W. Stinchomb, "A Critical Element Model of the Residual Strength and Life of Fatigue Loaded Coupons," *Composite Materials: Fatigue and Fracture*, ASTM STP 907, Edited by H. T. Hahn, ASTM, (1986), 298-303.
- [38] Case, S.W. and Reifsnider, K.L., MRLife11<sup>TM</sup> A strength and Life Prediction Code for Laminated Composite Materials, Materials Response Group, Virginia Tech, (1998).
- [39] Reifsnider, K.L., "Use of Mechanistic Life Prediction Methods for the Design of Damage-Tolerant Composite Material Systems," *Advances in Fatigue Lifetime Predictive Techniques: Second Volume*, ASTM STP 1211, (1993), pp. 3-18.
- [40] Reifsnider, K., Case, S., and Iyengar, N., "Recent Advances in Composite Damage Mechanics," Proceedings of Conference on Spacecraft Structures, Materials & Mechanical Testing (ESA SP-386), Noordwijk, The Netherlands, June 1996, pp. 483-490.
- [41] Schaff, J, "Life Prediction Methodology for Composite Laminates, Constant Amplitude and Two-Stress Level Fatigue" WL-TR-94-4046, Wright Laboratory Air Force Materiel Command, September 1994.
- [42] Kachanov, L. M., Introduction to continuum damage mechanics. Martinus Nijhoff Publishers, Boston. (1986).
- [43] Case, S., Iyengar, N., and Reifsnider, K., "Life Prediction Tool for Ceramic Matrix Composites at Elevated Temperatures," *Composite Materials: Fatigue and Fracture*, Seventh Volume, ASTM STP 1330, R. B. Bucinell, Ed., American Society for testing and Materials, 1998, pp. 165-178.

## **VITA**

Blair Edward Russell is the son of David and Raylene and brother to Erika. He was born in Honolulu, Hawaii on September 4, 1970. As the son of a Naval officer, he was soon off on a world tour. From Hawaii, he spent several years in Norfolk, Virginia, then a few in Misawa, Japan, a few in Monterey, California, and nine years in Manassas, Virginia at the end of which he graduated from Osborne Park High School. In the fall of 1989, Blair began his undergraduate education at Virginia Tech in the college of Engineering. After 4 semesters he found a home in the Engineering Science and Mechanics department. In the summer of 1995, Blair joined the Materials Response Group and after a few months started working on the Wellstream project. The initial work on this project served as his Senior Design Project and he graduated from the ESM department in 1996. Blair was admitted to the Engineering Mechanics Graduate program in the spring of 2000 and graduates with a Masters Degree in December of the same year.